Blossoming of the Pleistocene volcanism in the Ecuadorian Andes: a review based on new and recent geochronological data

Santiago Santamaría, Mathilde Bablon, Xavier Quidelleur, Pablo Samaniego, Jean-Luc Le Pennec, Silvana Hidalgo, Céline Liorzou

Blossoming of the Pleistocene volcanism in the Ecuadorian Andes: a review based on new and recent geochronological data

Santiago Santamaria [a,*], Mathilde Bablon [b], Xavier Quidelleur [a], Pablo Samaniego [c], Jean-Luc Le Pennec [d], Silvana Hidalgo [e], Céline Liorzou [d]

[a] GEOPS, Université Paris-Saclay, CNRS, Rue du Belvédère, 91405 Orsay, France

[b] Université Côte d'Azur, CNRS, IRD, Observatoire de la Côte d'Azur, Géoazur, Valbonne, France

[c] Laboratoire Magmas et Volcans, Université Clermont Auvergne, CNRS, IRD, OPGC, F-63000 Clermont-Ferrand, France

[d] Geo-Ocean, Univ Brest, CNRS, Ifremer, UMR6538, IRD, Institut Universitaire Européen de la Mer, 29280 Plouzané, France

[e] Instituto Geofísico, Escuela Politécnica Nacional, Ap. 17-01-2759, Quito, Ecuador

[*] corresponding author (email: ssantamaria@yachaytech.edu.ec; sdsantiago@gmail.com). Now at: School of Earth Sciences, Energy and Environment, Universidad Yachay Tech, Urcuquí, Ecuador.

Keywords:

- Volcanic arc
- Ecuador
- K-Ar dating
- Geodynamics
- Carnegie Ridge

Key Points:

- We have compiled a dataset of 250 ages from 45 volcanoes in Ecuador
- Oldest volcanism mostly occurred in the Eastern Cordillera of the Quito segment
- Since about 1.4 Ma volcanic activity spread around the Quito segment
- Volcanic activity increased extensively throughout the arc since ~600 ka
- The Carnegie Ridge subduction influenced the Ecuadorian volcanism evolution

Word count:

- Abstract: 348 words
- Main body: 10497 words

Figures: 12; Tables: 2; Appendices: 5

Submitted to Bulletin of Volcanology; April 2024

ABSTRACT

The Ecuadorian arc is composed of an unusually high number of volcanoes, organized as along-arc alignments and across-arc clusters, in a relatively small area. Although several geochronological studies have been carried out in the last three decades, the eruptive history of the central zone of the arc remains poorly documented, preventing analysis of the initiation of volcanism of the whole arc. In this study, we present new K-Ar ages obtained from this central area, referred to as the Quito segment. These results were then incorporated into an updated comprehensive geochronological database of about 250 ages, allowing us to describe, at the arc scale, the spatial and temporal evolution of Quaternary volcanism in Ecuador. About eighty Quaternary volcanoes have been identified in the Ecuadorian Andes, 45 of which have been radioisotopically dated and/or identified as active or potentially active. The volcanic arc developed in three stages, characterized by an increase in the total number of active volcanoes. During the oldest Plio-Early Pleistocene stage, documented volcanic activity was mostly concentrated in the Eastern Cordillera of the Quito segment, with minor effusive eruptions in the southern Back-Arc. Since ~1.4 Ma, activity has spread to the surroundings of the Quito segment, and new edifices also appeared in the Western Cordillera and the Inter-Andean Valley. Towards the end of this intermediate stage (i.e., ~800 ka), volcanism occurred in isolated areas north and south of the Inter-Andean Valley. Finally, the late and current has been characterized by a remarkable increase in volcanic activity since ~600 ka. About 50 volcanoes were active during this stage. The spatial distribution of the Ecuadorian arc volcanism seems to be guided by deep mechanisms (i.e., slab geometry and age, amount and composition (fluids and melts) of slab input, mantle heterogeneities) and old crustal tectonic structures of the Western Cordillera, while neotectonics seems to influence the development of stratovolcanoes. In addition, we note that the spatial and temporal evolution of volcanism highlights the influence of the Carnegie Ridge and the young Nazca crust on the thermal regime of the subduction system, which in turn increases of volcanic activity in Ecuador.

1. INTRODUCTION

The study of the evolution of a volcanic arc is essential for understanding the processes that control the spatial distribution of volcanoes, the dynamics of their eruptions, and therefore, the associated risks to populations and communities. Thus, improving the fundamental knowledge of the relationships between volcanism and geodynamics becomes a necessary step to establish monitoring strategies for active volcanoes. Here, we present the analysis of the spatial and temporal evolution of Ecuadorian volcanoes, providing valuable insights into their relationship with the crustal structures and the slab configuration.

The Northern Andean Volcanic Zone results from the subduction of the oceanic Nazca plate beneath the northwestern margin of the continental South American plate (Fig. 1a; Hall and Wood, 1985). The volcanic activity in Ecuador developed over a large area, up to 270 km wide, and produced about eighty Quaternary volcanoes (Hall and Beate, 1991; Hall et al., 2008; Ramon et al., 2021). The recent eruptive activity of the Tungurahua, Pichincha, and El Reventador volcanoes during the 2000s highlighted the need to improve the knowledge of the evolution of Ecuadorian volcanoes and thus the associated volcanic hazard assessment. Therefore, several vulcanological, geochronological, geochemical, petrological, and geophysical studies have been carried out in the Ecuadorian Andes (e.g., Hall and Mothes, 2008a; Robin et al., 2010; Le Pennec et al., 2011), focusing mainly on volcanoes that were "active" during the Holocene or with morphological features suggesting "potential" Holocene activity (Hall and Beate, 1991). These studies revealed that at least twenty Ecuadorian volcanoes were active during the Holocene (e.g., Samaniego et al., 1998; Barba et al., 2008; Hall et al., 2008; Hidalgo et al., 2008; Robin et al., 2008; Bernard et al., 2014). Their activity resulted in the formation of thick volcaniclastic sequences that are now overlain by heavily populated areas, including the capital of Ecuador, Quito (Hall and Mothes, 2008b). Several authors have also suggested a possible link between the spatial distribution of volcanism and its geochemical variability in relation to the subduction of the Carnegie Ridge, crustal tectonics and the slab geometry (e.g., Litherland and Aspden, 1992; Barberi et al., 1988; Gutscher et al., 1999; Samaniego et al., 2002, 2005; Bourdon et al., 2003; Garrison et al., 2006; Chiaradia et al., 2009, 2021; Hidalgo et al., 2012; Ancellin et al., 2017).

Recently, several geochronological studies have shed light on the development of the Quaternary volcanism in Ecuador, with emphasis on the southern termination of the arc and its central and northern segments (e.g., Alvarado et al., 2014; Bablon et al., 2019, 2020a; Santamaría et al., 2023). In this work, in addition to compiling radioisotopic ages at the arc scale, we focus on the central zone of the arc, which has a relatively limited number of dated volcanic complexes. We present twelve new K-Ar ages obtained from ancient edifices from the Quito segment. This allows us to clarify the eruptive history of volcanoes from this densely populated area, and to provide new ages to expand the radioisotopic age dataset. We have also carefully selected and compiled the available geochronological data for the Pleistocene volcanism in Ecuador to present the first summary of the eruptive history of the whole volcanic arc based on K-Ar, $^{40}Ar/^{39}Ar$, and fission track ages.

2. GEOLOGICAL CONTEXT

2.1. Ecuadorian geological setting

Physiographically, Ecuador is composed of the Coastal Forearc and the Oriente Foreland basins separated by the Andes Mountains. The northern Ecuadorian Andes are divided into two parallel ranges, known as the Western and Eastern Cordilleras, with the Inter-Andean Valley between them (Fig. 1b). The basement lithologies and ages in these domains are widely variable (Egüez et al., 2017; Jaillard, 2022). For instance, the Coastal basin and the Western Cordillera are formed by Cretaceous MORB-like basalts accreted during the Late Cretaceous-Paleogene, overlain by Tertiary marine sediments and volcaniclastic deposits (Jaillard et al., 2004; Witt et al., 2019; Vallejo et al., 2019). Conversely, the Eastern Cordillera is composed of Paleozoic to Jurassic metamorphic rocks, mostly of continental affinity, and felsic to mafic igneous rocks (Litherland et al., 1994; Spikings et al., 2015; Villares et al., 2020). The Inter-Andean Valley is composed of Miocene-Pleistocene volcanic sediments that overlie a tectonic *mélange* of continental and oceanic rocks derived from both cordilleras (Aspden et al., 1995; Lavenu et al., 1995; Winkler et al., 2005). The basement of the Oriente basin corresponds to the Pre-Cambrian Guyanese craton, overlain by a thick Mesozoic to Cenozoic sedimentary sequence

(Ibanez-Mejia et al., 2011; Baby et al., 2013; Gutiérrez et al., 2019; Vallejo et al., 2021). The Miocene-Pliocene volcanic activity formed thick volcanic sequences (Lavenu et al., 1995; Vallejo et al., 2019, 2020; Chiaradia et al., 2021), presently exposed over both cordilleras, on which part of the Pleistocene-Holocene volcanic edifices developed. The thickness of the continental crust is estimated to be ~55-60 km for both the Western and Eastern Cordilleras (e.g., Koch et al., 2021).

Subduction of the oceanic Nazca plate led to the development of the Ecuadorian volcanic arc (Hall and Wood, 1985; Barberi et al., 1988). The Grijalva Fracture Zone (Fig. 1a), which resulted from the fragmentation of the ancient Farallon plate during the Early Miocene (~22-23 Ma), divides the Nazca plate into two distinct crusts, issued from the Galápagos spreading center to the north, and from the East Pacific rise to the south. Moreover, the eastward motion of the Nazca plate over the Galápagos hotspot led to the formation of the Carnegie Ridge, a 300 km-wide submarine mountain range built on the younger Nazca crust (Meschede and Barckhausen, 2000; Lonsdale, 2005; O'Connor et al., 2007). The complex structure of the Nazca plate and its corresponding thermal state affect the buoyancy of the subducted slab, which is then reflected in a change in dip angle from ~12° for the older crust (south of the GFZ) to >22° for the younger crust (north of the GFZ). This difference in subduction angle, combined with the convex shape of the continental margin, has induced a slab flexure beneath the southern part of the Ecuadorian Andes (Fig. 1a; Yepes et al., 2016; Portner et al., 2020; Araujo et al., 2021). The presence of the Carnegie Ridge has also been associated with notable variations in the nature of the metasomatic agent of the sub-arc mantle wedge. This agent has been postulated to be an aqueous fluid resulting from slab dehydration reactions, with variable inputs of a siliceous melt associated with partial melting of both the sedimentary and basaltic portions of the subducted slab (e.g., Barragan et al., 1998; Bourdon et al., 2003; Hidalgo et al., 2012; Ancellin et al., 2017; Narvaez et al., 2018). As previously proposed, partial melting of the slab could be associated with an increase in the thermal regime related to the presence of the Carnegie Ridge, changes in slab geometry, and/or differences in slab ages and rheology (e.g., Yepes et al., 2016; Ancellin et al., 2017; Narvaez et al., 2018). These issues could also influence the spatial configuration of the volcanic arc (Bablon et al., 2019, 2020a).

Furthermore, the oblique convergence of the Nazca Plate caused the motion of the northwestern edge of the South American plate known as the North Andean Sliver (Fig. 1a). The southeastern limit of its deformation zone corresponds to the Chingual-Cosanga-Pallatanga-Puná (CCPP) fault system. The CCPP fault system begins in the Gulf of Guayaquil, intersects the Ecuadorian Andes near the southern termination of the volcanic arc, and continues northward along the eastern edge of the Eastern Cordillera (Fig. 1; Witt and Bourgois, 2010; Alvarado et al., 2014; Nocquet et al., 2014; Jarrin et al., 2023).

2.2. Overview of the Ecuadorian volcanic arc

Quaternary volcanism in Ecuador is characterized by a wide variety of well-preserved volcanic morphologies related to multiple eruptive styles and magmatic compositions. The resulting structures typically correspond to prominent composite cones with basal diameters of several kilometers, usually greater than 7 km (e.g., Cotopaxi volcano; Hall and Mothes, 2008a). Successive conduit migrations and/or changes in eruptive styles caused the superposition of edifices. Such events gave rise to large volcanic complexes or compound volcanoes, which are the most common structures observed in the Ecuadorian Andes (e.g., Pichincha volcanic complex; Robin et al., 2010). The construction processes of these "edifices" have also been interrupted by sector collapses, separating their eruptive histories into distinct cone-building stages (e.g., Tungurahua volcano; Hall et al., 1999; Bablon et al., 2018). Conversely, highly explosive eruptions have resulted in the formation of large calderas (e.g., Chalupas caldera; Beate, 1985; Bablon et al., 2020b). Also, less prominent structures such as lava domes (e.g., Pululahua dome complex; Andrade et al., 2021) and monogenetic cones with their corresponding lava flows (e.g., Tulabug cone; Bablon et al., 2019) have also been identified.

The Ecuadorian arc is usually described in terms of the geographic distribution of its numerous volcanoes along NNE-SSW alignments roughly parallel to the trench (e.g., Hall, 1977; Hall and Beate, 1991). These volcanoes built on oceanic basement (Western Cordillera and eastern Inter-Andean Valley) roughly constitute the Volcanic Front (yellow volcanic centers, Fig. 2), whereas those built on

continental basement (western Inter-Andean Valley and Eastern Cordillera) are called the Main Arc (orange and purple volcanic centers, Fig. 2). The Back-Arc volcanoes are located in the Sub-Andean zone (blue volcanic centers, Fig. 2). The magmas in each of these regions have distinctive geochemical and petrographic characteristics that lead to different eruptive styles and volcanic landforms (Hall et al., 2008; Ancellin et al., 2017). Notably, the along-arc distribution of these volcanoes is not uniform. For sake of clarity, we have divided the Ecuadorian arc into ~50 km-long segments perpendicular to the axis of the Volcanic Front (Fig. 2). Note that the boundaries of these segments roughly coincide with the Chota, Guayllabamba, Latacunga, and Riobamba valleys, where a smaller number of volcanoes are observed. The volcanoes located in the Tulcán, Ibarra, Machachi, and Ambato segments form across-arc "volcanic clusters" that include various composite stratovolcanoes and lava dome complexes. In these areas, the distance between volcanic summits ranges only from ~7 to ~15 km. These volcanic clusters cover areas of a few hundred square kilometers. We note that despite the short distance between volcanoes, their eruptive products show a wide geochemical variability resulting in multiple eruptive styles.

The volcanic products of the Ecuadorian arc have been classified as medium to high potassium calc-alkaline basaltic andesites to rhyolites (e.g., Hall et al., 2008; Hidalgo et al., 2012; Ancellin et al., 2017; Chiaradia et al., 2020), with exceptional occurrences of shoshonitic rocks in Back-Arc setting (e.g., Bourdon et al., 2003; Hoffer et al., 2008; Garrison et al., 2017). Overall, the concentrations of incompatible elements (e.g., K, Rb, Sr, Ba, La, Th) tend to increase with distance from the trench. Furthermore, a decrease in the concentrations of elements considered fluid-mobile (e.g., Ba, Pb, Cs, Li, B) relative to fluid-immobile elements (e.g., Be, Nb, Th, La) has been observed with increasing distance from the trench (e.g., Barragan et al., 1998; Bryant et al., 2006; Chiaradia et al., 2009; Hidalgo et al., 2012; Ancellin et al., 2017).

2.3. Volcanism in the Quito segment

The Quito segment includes the volcanoes located approximately between 0° and 0.4° S latitude (Fig. 2). Our study focuses on the volcanoes surrounding the Guayllabamba valley, where few ages are available (Fig. 3). Volcanoes in the Sub-Andean zone (e.g., Hoffer, 2008; Mothes and Hall, 2008a; Salgado et al., 2021) were excluded due to the limited access roads and rainforest cover, which preclude adequate sampling. A summary of the geological background for the volcanoes in the Quito segment is provided below.

Pululahua (3357 m asl.; lat. 0°05'N; long. 78°49'W) is a dacitic dome complex, mostly formed during the Holocene, located on the axis of the eastern edge of the Western Cordillera. Recent activity at Pululahua (2.3 - 2.6 cal ka BP; Papale and Rosi, 1993; Andrade et al., 2021) included several highly explosive events (VEI 4) that produced a caldera-like depression and culminated in the extrusion of several dacitic lava domes within the caldera (Andrade et al., 2021). Southward, the **Casitagua** volcano (3519 m asl.; lat. 0°33'S; long. 78°48'W) is formed by a sequence of andesitic lavas interbedded with pyroclastic deposits. These volcanic successions are overlain by the lacustrine sediments of the San Miguel Formation (Pacheco et al., 2014) and the Cangahua Formation, an Upper Pleistocene, mostly reworked, highly altered volcanic formation composed of tephra fallout and flow deposits (Clapperton, 1990; Hall and Mothes, 1997). This sequence is deformed by the Quito fault system. The summit area of Casitagua currently shows a 5 km-diameter horseshoe-shaped structure containing several dacitic lava domes. Multiple domes also occur to the east and southwest of Casitagua volcano. The Catequilla and Pacto satellite lava domes are interspersed among the Casitagua volcanic sequences. They have been dated at 833 ± 26 ka and 898 ± 15 ka using the K-Ar Cassignol-Gillot technique applied to groundmass and plagioclase phenocrysts, respectively (Pacheco, 2013; Alvarado et al., 2014). An imprecise whole-rock K-Ar age of 1400 ± 1400 ka was provided for the Lulunurcu satellite dome by Geothermica Italiana (1989).

Further south, the **Pichincha volcanic complex** (4776 m asl.; lat. 0°17'S; long. 78°60'W) is formed by three superimposed edifices (Robin et al., 2010). The Cinto edifice, dated by $^{40}Ar/^{39}Ar$ at 1112 ± 24 ka, is the oldest edifice in the complex. It was later intruded by the Ungi lava dome, dated at 864 ± 48 ka. The Rucu Pichincha edifice is mainly composed of successions of andesitic lavas and

breccias formed between ~850 and ~262 ka, which partially cover the Cinto edifice. Further west, the Guagua Pichincha edifice, which is mostly dacitic in composition, rests on the western side of the Rucu Pichincha edifice. Its construction began as early as 52 ± 4 ka, and its most recent activity occurred between AD 1999 and 2001. Notably, several sector collapses have occurred during the eruptive history of Pichincha volcano (Robin et al., 2010). South of the El Cinto edifice lies La Carcacha volcano (3880 m asl.; Lat. 0°19'S; Long. 78°36'W), an old edifice (~1290 ka; Hidalgo, 2006) of the **Atacazo-Ninahuilca volcanic complex** (4455 m asl.; lat. 0°36'S; long. 78°62'W). The main cone-building stages of Atacazo occurred between ~220 and ~83 ka, followed by the extrusion of several satellite domes around ~71 ka and the Holocene high-explosive activity (VEI 4 or higher) of the Ninahuilca lava dome complex (Hidalgo, 2006; Santamaría et al., 2023). **Ilaló** (3188 m asl.; lat. 0°26'S; long. 78°42'W) is the only volcano in the Inter-Andean Valley within the study area. This highly eroded volcano is formed by sequences of andesitic lavas (Chiaradia et al., 2009) overlain by the Cangahua Formation. A whole-rock K-Ar age of 1620 ± 160 ka was obtained for a basaltic andesite lava (Barberi et al., 1988), although the location of the sampling site is not reported.

Several highly eroded volcanoes dominate the western edge of the Eastern Cordillera. To the north of the study area, **Pambamarca** volcano (4078 m asl.; lat. 0°08'S; long. 78°21'W) is formed by voluminous andesitic lava sequences overlain by a complex of dacitic and rhyolitic domes. Herradura is a *dome coulée* located in the summit area that, unlike most of Pambamarca's structures, shows scarce signs of erosion. Further south, **Cerro Puntas** (4558 m asl.; lat. 0°19'S; long. 78°21'W) is a volcano composed of sequences of monolithological breccias and lavas surrounded by incised glacial valleys. The southwestern flank of Puntas volcano partially covers the smaller **Coturco** volcano (3572 m asl.; lat. 0°21'S; long. 78°28'W), also called Cotohurcu or Leon Dormido (Bernard and Andrade, 2011). To the east, the **Chacana** caldera (4493 m asl.; Lat. 0°21'S; Long. 78°15'W) dominates the Eastern Cordillera, occupying an area 32 km long (N-S) and 20 km wide (E-W). The oldest volcanic products of Chacana are dated by $^{40}Ar/^{39}Ar$ between 2150 ± 200 and 2710 ± 190 ka (Opdyke et al., 2006). The caldera-forming episode involved the emission of voluminous ignimbrite flows that spread radially along the caldera flanks, forming the Quiscatola-Yanaurcu and Tablones series. These sequences are

dated by obsidian fission-tracks between 1350 ± 90 and 1580 ± 70 ka, and at 810 ± 50 ka, respectively (Bellot-Gurlet et al., 2008). Two $^{40}Ar/^{39}Ar$ ages are provided for the Quiscatola-Yanaurcu series at 1670 ± 190 and 1460 ± 50 ka (Opdyke et al., 2006). Alternatively, two glass K-Ar ages of 980 ± 13 and 810 ± 40 ka are consistent with the range of the Tablones series, although the sampling locations are not indicated (Barberi et al., 1988). The plateau created by these deposits surrounds the Pambamarca, Puntas and Coturco volcanoes. The subsequent Chacana activity phase corresponds to the uplift of the caldera floor caused by a shallow intracaldera intrusion (post-collapse resurgence stage), followed by a highly explosive episode and the emplacement of rhyolitic lava domes (Hall and Mothes, 2008c; Beate et al., 2010). The volcanic products of these episodes are dated between 450 and 160 ka (Opdyke et al., 2006; Bellot-Gurlet et al., 2008). The most recent major eruptions produced two 8 m-thick regional pumice-fallouts. The associated rhyolitic lava domes have been dated at 180 ± 20 and 170 ± 10 ka (Bigazzi et al., 2005). More recently, several andesitic and dacitic lava flows have been erupted, including the fissure eruptions of Pinantura (AD 1728) and Papallacta (AD 1773).

A sequence of voluminous andesitic lavas forms the northern flank of the Chacana caldera. These lava flows are associated with the **Izambi** volcano (4325 m asl.; Lat. 0°19'S; Long. 78°17'W), also called Gualimburo (Aguilera et al., 2007). Some authors consider this voluminous sequence to be part of the Chacana series, while the upper lava sequence (Pucará Chico peak) is assigned to the Izambi volcano (e.g., Hall and Mothes, 2008c; Bernard and Andrade, 2011). A basaltic andesitic lava was dated at 1300 ± 200 ka by whole-rock K-Ar (Barberi et al., 1988). Although the sampling location is not provided, the sample may correspond to the most accessible Gualimburo series. Alternatively, an obsidian block sampled near the Pucará Chico peak yielded a fission-track age of 370 ± 60 ka (Bigazzi et al., 2005).

3. METHODS

3.1. Sampling strategy

Sampling lavas for geochronology from the Quito Segment was carried out in 2020. Fresh lavas with low vesicle contents were sampled for K-Ar dating and whole-rock major and trace element analyses. Where possible, outcrops in both the summit and basal areas of the volcanic edifices were targeted (Fig. 3) in order to bracket the whole eruptive history of the studied volcanoes.

At Casitagua volcano, two samples were collected from massive andesitic lava flows located on its southern (20EQ51a) and western (20EQ52a) flanks. Three juvenile blocks (20EQ51b, 20EQ52b, 20EQ52c) were sampled from pyroclastic density current (PDC) deposits overlying the previously sampled lavas for geochemical comparison. A dacitic dome located within the horseshoe-like depression was also sampled (20EQ53). At Ilaló volcano, three massive lava flows were sampled at the base (19EQ01) and in the summit area (19EQ47, 19EQ48). The overlying thick deposits of the Cangahua Formation preclude the exposure of multiple outcrops on these volcanoes and thus prevented additional sampling.

Eight samples were collected from Pambamarca volcano. Four samples correspond to andesitic lavas located on the northern flank (20EQ56) and the summit area (20EQ59, 20EQ60, 20EQ61). Four samples were collected from the summit rhyolitic domes of Herradura (20EQ57, 20EQ58), Jambi Machay (20EQ62) and Quito Loma (20EQ63) (Fig. 3b). Only the northern flank of Puntas volcano was sampled due to poor access routes. However, four massive lavas were sampled at different elevations (20EQ64, 20EQ65, 20EQ67, and 20EQ68). Likewise, only two lavas could be sampled in the summit area of Coturco volcano (20EQ54, 20EQ55). Finally, we sampled a lava from the basal sequence on the southern side of the Antisanilla valley (20EQ85), located on the southern flank of the Chacana caldera.

3.2. K-Ar dating

Twelve samples were carefully selected for radioisotopic dating after thin-section examination (photographs available in Appendix A). We used the K-Ar dating method applying the unspiked Cassignol-Gillot technique (Gillot et al., 2006), which has been successfully applied previously to the Ecuadorian volcanic arc (Alvarado et al., 2014; Bablon et al., 2018, 2019, 2020b; Santamaría et al.,

2022, 2023), as well as to subduction and hotspot volcanism worldwide (e.g., Grosse et al., 2018, 2020; Hildenbrand et al., 2018; Dibacto et al., 2020). The Cassignol-Gillot technique is particularly suitable for dating volcanic rocks with low radiogenic argon (^{40}Ar*) contents diluted by atmospheric ^{40}Ar, such as young Low-K lavas found in the Ecuadorian arc. Using a 180° sector multi-collector mass spectrometer, the electrical signals measured for the ^{40}Ar and ^{36}Ar extracted from a given sample are compared with those from an air aliquot measured under identical pressure conditions. The difference in the measured ratios allows determination of the ^{40}Ar* produced by radioactive decay of ^{40}K since closure of the sample. The ^{40}Ar signal is calibrated by systematic measurements of the HD-B1 standard (24.18 ± 0.09 Ma; Schwarz and Trieloff, 2007) to convert the electrical signals into a certain number of atoms. Thus, the argon measurement process depends solely on the ^{40}Ar* content of the sample, whose electrical signal is optimized by adjusting the initial sample mass. The measurement process was carried out at the GEOPS laboratory of the Université Paris-Saclay (France), where the detection limit of the mass spectrometer is close to 0.1% for ^{40}Ar* (Quidelleur et al., 2001), allowing the dating of Holocene volcanic rocks with relatively low uncertainty (Gillot et al., 2006). The potassium (K) concentration is measured independently by flame absorption spectroscopy. MDO-G (Gillot et al., 1992) and BCR-2 (Raczek et al., 2001) standards are measured together with the analyzed samples for sake of comparison and correction purposes. Finally, the age is calculated from the ^{40}K/K ratio in nature, the ^{40}K to ^{40}Ar decay constant (Steiger and Jäger, 1977), and the measured K and ^{40}Ar* contents. The reproducibility of the measurements was verified within a 1-σ uncertainty range by replicating the whole process at least twice for each sample.

We prefer to apply this technique to the groundmass because it is the last phase to crystallize in equilibrium with the atmosphere after magma eruption. Phases crystallized before eruption, such as plagioclase phenocrysts, may carry inherited radiogenic argon biasing the calculated ages (e.g., Singer et al., 1998; Samper et al., 2008). Therefore, we consider K-Ar ages performed on crystals or whole-rock as older bounds of the real eruption date. To separate groundmass and crystal phases, samples were hand crushed and sieved to 63-80, 80-125 or 125-250 μm, depending on the average distance between phenocrysts occupied by groundmass. Subsequently, dilute acid (10% HNO_3) leaching, magnetic and

heavy-liquid (bromoform) separation procedures ensured that the recovered groundmass fraction remained homogeneous within a narrow density range and did not contain undetected weathered fractions. A full description of the sample preparation, analytical procedures, and age and uncertainty calculations can be found in Bablon et al. (2018).

3.3. Whole-rock geochemical analyses

Agate-crushed powders of all dated samples, together with 13 additional samples, were analyzed by Inductively Coupled Plasma-Atomic Emission Spectrometry (ICP-AES) following the analytical procedure described in Cotten et al. (1995) to determine their major and trace element contents. The relative uncertainties are < 1% for SiO_2, < 2% for other major elements, and < 5% for trace elements. The measuring process was carried out at the Laboratoire Geo-Ocean, Université de Bretagne Occidentale (France). The full dataset of 25 new whole-rock analyses is presented in Appendix B, where major element concentrations have been recalculated to a total of 100% on a water-free basis.

4. RESULTS

4.1. K-Ar dating

The samples selected for K-Ar dating show porphyritic to aphanitic textures with a mineral assemblage composed of plagioclase, orthopyroxene, clinopyroxene and amphibole crystals (Appendix A). Samples 20EQ62 and 20EQ63 from the summit domes of Pambamarca contain scarce biotite, while sample 20EQ63 contains unusually high amounts of orthopyroxene, amphibole, and biotite. The groundmass is generally composed of plagioclase, pyroxene, and scarce Fe-Ti oxide microlites hosted in a glassy matrix. Radioisotopic measurements were performed on groundmass only, except for samples 20EQ62, where plagioclase phenocrysts were used due to the intense alteration of the groundmass, and 20EQ54, where both groundmass and plagioclase phenocrysts were analyzed. K contents range from 0.964% to 1.411% for the groundmass and from 0.382% to 1.141% for the

plagioclases (Table 1). The minimum $^{40}Ar^*$ content is 6.7%, registered in sample 19EQ47 sample, with a mean of about 21%. Note that although the plagioclase fractions contain lower amounts of K, the $^{40}Ar^*$ content is significantly higher than the detection limit (Quidelleur et al., 2001), allowing accurate and reliable age determination using the Cassignol-Gillot technique.

Twelve new K-Ar ages are presented in Table 1 and Figure 3. Samples from Casitagua volcano yield ages of 785 ± 16 ka (20EQ51a) and 878 ± 13 ka (20EQ52a; Fig. 3a). A narrower age range of 1273 ± 20 ka (19EQ01) and 1112 ± 22 ka (19EQ47) is obtained for Ilaló volcano. Further east, two andesitic lavas from Pambamarca volcano are dated at 1261 ± 18 ka (20EQ60) and 1374 ± 21 ka (Fig. 3b; 20EQ56). Due to the highly weathered state of the groundmass phases observed in the summit lava dome samples from Pambamarca volcano, we analyzed plagioclase phenocrysts and obtained an age of 1292 ± 20 ka for the Jambi Machay dome (20EQ62; Fig. 3b). Three ages at 1084 ± 17 ka (20EQ67b), 1128 ± 16 ka (20EQ68), and 1132 ± 16 ka (20EQ66) were obtained for Puntas volcano (Fig. 3c). Due to the limited number of samples from Coturco volcano and the slight evidence of weathering, the measurements were performed on both groundmass and plagioclase phenocrysts extracted from the freshest sample 20EQ54. The calculated values were consistent within the 1-sigma uncertainty range, yielding a mean age of 1959 ± 28 ka (Fig. 3c). Finally, the lava from the old Chacana series sampled in the Antisanilla valley was dated at 2228 ± 34 ka (20EQ85; Table 1, Fig. 3a).

4.2. Geochemical characterization

Figures 4a and 4b show the Peccerillo and Taylor (1976) rock classification diagram for the samples collected in this study. Most of the samples are Low to Medium-K basaltic andesites and andesites with SiO_2 contents ranging from 53 to 63 wt.%, and K_2O contents ranging from 0.7 to 2.5 wt.%. Samples collected on the Casitagua volcano plot in the field displayed by the PDC deposits associated with this edifice (yellow symbols and fields, Fig. 4 a, b), sampled in the Quito basin, east of the Monjas river (Fig. 3a). Note that data from the Catequilla dome, located northeast of Casitagua (Fig. 3a), are also plotted in the same Casitagua PDC field (Pacheco, 2013). The andesitic lavas from

Ilaló volcano lie in the field described in previous studies (Chiaradia et al., 2009), except for sample 19EQ47, which has a lower silica content (red symbols and fields, Fig. 4b). Sample 20EQ85 form the old Chacana series is a basaltic andesite that plots outside the Chacana field (e.g., Chiaradia et al., 2009, 2014; Villares, 2010), although it appears to be consistent with the overall volcano trend (green symbols and fields, Fig. 4a, b). The samples from the Jambi Machay (20EQ62) and Quito Loma (20EQ63) summit domes of Pambamarca volcano are the only Medium-K rhyolites identified in this study (purple symbols, Fig. 4a). The samples from the Herradura dome (20EQ57 and 20EQ58) exhibit an unusual K_2O enrichment at low SiO_2 content, which classifies them as basaltic andesites belonging to the Shoshonitic series, which are quite common in Back-Arc volcanoes (e.g., Hoffer et al., 2008; Garrison et al., 2017).

Rare-Earth Elements (REE) normalized to chondrite and spider diagrams of trace elements normalized to the primitive mantle are shown in Figures 4c and 4d, respectively. In summary, these diagrams show fractionation between Light REE (LREE; e.g., La, Ce) and Heavy REE (HREE; e.g., Yb) with a slightly declining but homogeneous pattern, with no Eu anomaly observed for Casitagua, Ilaló, Puntas and Coturco volcanoes. A slight increase in REE concentration is observed between the Volcanic Front (Casitagua), Inter-Andean Valley (Ilaló) and the Main Arc (Puntas, Coturco), indicating a positive correlation between REE contents and distance from the trench (Fig. 4c-d), as previously documented at the arc scale (e.g., Ancellin et al., 2017). Sample 20EQ48 from Ilaló volcano distinguishes with significantly higher contents in most REE. The lavas of Pambamarca volcano exhibit a wide range of REE contents, with the andesitic samples, the summit rhyolitic domes, and the Herradura dome defining compositional fields consistent with those found in the Chacana caldera. In particular, the Herradura dome (20EQ57, 20EQ58) shows the highest REE enrichment of the whole dataset, creating a pattern remarkably similar to the Yuyos lava flow from the Chacana caldera (Fig. 3a; Chiaradia et al., 2014). Other lavas with similar petrographic and geochemical characteristics occur at Cayambe (Cono La Virgen; Samaniego et al., 2005) and Antisana (Cuyuja lavas; Hall et al., 2017) volcanoes. The primitive mantle-normalized trace element patterns reveal an overall enrichment in Large-Ion Lithophile Elements (LILE; e.g., Rb, Ba). A negative Nb anomaly is observed for the whole

dataset (Fig. 4d), typical of arc magmas. Only samples from the Jambi Machay (20EQ62) and Quito Loma (20EQ63) domes show significant negative P and Ti anomalies. These domes also have the highest depletions of Dy, Y and Yb (Fig. 4d).

5. DISCUSSION

5.1. Comparison between new and previous ages from the Quito segment

Overall, our new K-Ar ages are in agreement with previously published studies. The Catequilla and Pacpo domes, located northeast and southeast of Casitagua volcano (Fig. 3a), were previously dated between 833 ± 26 and 898 ± 15 ka using the same unspiked K-Ar method (Pacheco, 2013; Alvarado et al., 2014). We dated two andesitic lava flows sampled on the flanks of Casitagua volcano and obtained close ages of 785 ± 16 and 878 ± 13 ka (20EQ51a and 20EQ52a, respectively; Fig. 3a). These new data suggest that the eruptive activity of Casitagua was contemporaneous with the emplacement of the Catequilla and Pacpo satellite domes. Furthermore, this period of eruptive activity is stratigraphically consistent with the K-Ar age of 1152 ± 30 ka obtained from the underlying basaltic andesite lavas assigned to the Pisque Formation (Fig. 3a; Alvarado et al., 2014).

In the Inter-Andean Valley, groundmass ages acquired from the Ilaló volcano suggest an activity between 1112 ± 22 and 1273 ± 20 ka (19EQ47 and 19EQ01, respectively; Table 1). This range is younger than the rather poorly constrained whole-rock K-Ar age of 1620 ± 160 ka previously reported (EC 76; Barberi et al., 1988). Although the exact sampling location of EC 76 was not provided, it appears to correspond to the lava 19EQ01, located in an easily accessible outcrop on the northwestern flank of Ilaló (Fig. 3a; P. Mothes, pers. comm.). We interpret the age difference to be due to (1) the presence of phenocrysts within the whole-rock fraction that may carry inherited argon; and/or (2) the inclusion of weathered grains for which potassium may have partially leached out (e.g., Samper et al., 2008; Schaen et al., 2020). Note that such a bias toward older ages has already been noted for other lavas in the Ecuadorian arc dated on whole-rock fractions (e.g., Bablon et al., 2018, 2019) and elsewhere (e.g., Quidelleur et al., 1999, 2021; Samper et al., 2008).

The ages obtained in this study were not biased by differences in the ratio of microcrystals to glass in the groundmass. Samples from the Ilaló volcano, for instance, contain different amounts of glass in their groundmass. Sample 19EQ01 has a groundmass rich in microcrystals (80%), while sample 19EQ47 has lower amounts of crystals (60%). However, the ages of both samples (1273 ± 20 ka and 1112 ± 22 ka, respectively) are consistent with their relative stratigraphic position. Similar statements can be made for other volcanoes described here or in other studies (e.g., Bablon et al., 2018, 2020a; Santamaría et al., 2022; Santamaria et al., 2023; Almeida et al., 2023). Note that vitreous samples, including obsidians and pumices, have also been successfully dated in agreement with stratigraphy and with ages provided by other dating techniques (e.g., Bablon et al., 2020b; Santamaria et al., 2023).

5.2. Geochronological data compilation of the Ecuadorian volcanic arc

In order to constrain the onset of eruptive activity of the current Ecuadorian arc, we have compiled available geochronological data for Ecuadorian volcanoes (Fig. 5). Note that ^{14}C ages are not considered here because they have been largely used for the detailed study of the recent eruptive history of volcanism in Ecuador, due to their limitation to about 50 ka towards their older bound. Nevertheless, a compilation of these data is offered in Santamaría (2017). Low quality data, such as whole-rock K-Ar ages, have been discarded (see section 5.1). Similarly, $^{40}Ar/^{39}Ar$ ages without minimum quality criteria, such as plateau ages calculated with at least three consecutive steps corresponding to at least 50% of the total ^{39}Ar released, and having an associated isochron with an initial $^{40}Ar/^{36}Ar$ ratio indistinguishable from the atmospheric value (e.g., Fleck et al., 1977), have also been removed. Finally, following Ramon et al. (2021), we considered volcanic systems to be "potentially active" or "active", if there was evidence of Holocene or historical activity, respectively (Table 2).

We followed the approach of considering eruptive subsystems that show spatial and/or temporal overlap (e.g., Rucu Pichincha and Guagua Pichincha volcanoes) as a single volcano (e.g., Pichincha volcanic complex; Robin et al., 2010). A thorough bibliographic review led to the identification of 78 individual volcanic systems in the Ecuadorian arc (Appendix C), 45 of which have published

radioisotopic ages in the Ecuadorian arc (Table 2). This database includes nearly 250 ages (Appendix C), with 145 recent K-Ar ages obtained on groundmass (Fig. 5; Alvarado et al., 2014; Telenchana et al., 2017; Bablon et al., 2018, 2019, 2020a, 2020b; Andrade et al., 2021; Santamaría et al., 2022, 2023; this study; Almeida et al., 2023), 89 $^{40}Ar/^{39}Ar$ ages measured on groundmass or separated crystalline phase (e.g., Monzier et al., 1999; Hammersley, 2003; Samaniego et al., 2005; Hidalgo, 2006; Opdyke et al., 2006; Hoffer, 2008; Hoffer et al., 2008; Hall et al., 2017; Robin et al., 2010; Le Pennec et al., 2011; Bellver-Baca et al., 2020), as well as 15 fission track ages (e.g., Bigazzi et al., 1992, 2005; Bellot-Gurlet et al., 2008).

5.3. Pleistocene eruptive history of the Ecuadorian arc

Figure 6 shows the timing of activity based on the radioisotopic ages database presented above (Appendix C) and summarized in Table 2, as well as stratigraphic and morphological data. Remarkably, the volcanic activity was not uniformly distributed in space and time. Based on the number of active volcanoes, three time-intervals of volcanic activity can be identified from Figure 6, with an early stage older than 1.4 Ma, an intermediate stage between 1.4 and 0.6 Ma, and a late stage for activity younger than 0.6 Ma. Accordingly, a summary of the Pleistocene eruptive history of the Ecuadorian arc is presented below.

5.3.1. Early stage: > 1.4 Ma

The few oldest available ages provide evidence for volcanic activity occurring from at least 2.5 and up to 1.4 Ma in the Quito and Ambato-Latacunga segments (dark yellow fields, Fig. 7). Note that the occurrence of coeval activity in other segments cannot be excluded due to sampling bias towards the most recent units and the limited number of published studies focusing on Early Pleistocene volcanism. In addition, the gradual erosion of the oldest deposits and their coverage by younger products prevents us from defining a precise age for the onset of the arc construction, although geochronological data seem to point to ~2.5 Ma.

Quito segment

$^{40}Ar/^{39}Ar$ plateau ages reported for the **Chacana** caldera (Western Cordillera) suggest that active volcanism occurred in the center of the present-day Chacana caldera at ~2.6 ± 0.2 Ma (Opdyke et al., 2006). We have obtained here a consistent, albeit much more precise, K-Ar age of 2228 ± 34 ka (20EQ85; Table 1) for a basal lava flow that forms the southern flank of the caldera. To the east, the construction of **Coturco** volcano appears to be contemporaneous with this early stage of Chacana, as suggested by our K-Ar age of 1959 ± 28 ka (20EQ54; Table 1) acquired from a summit lava flow. No additional age from this period has been reported for the Western Cordillera or the Sub-Andean zone in the Quito segment.

Coeval activity in the Ambato and Latacunga segments (Back-Arc)

The low-volume, mostly effusive volcanism that occurred in the Sub-Andean zone formed several cone-shaped landforms of a few tens of meters height (Cacalurco and Chuvaurcu cones), as well as thin lava sequences south of the town of Puyo (Hoffer et al., 2008; Ball, 2015). A $^{40}Ar/^{39}Ar$ age of 2770 ± 20 ka was obtained from the northern cone of **Cacalurcu** volcano (Fig. 7; Hoffer et al., 2008). Note that intense erosion and scarce exposures prevented accurate mapping in this zone. To the north of Puyo, a lava sequence identified as "**Mera Lavas**" was dated by $^{40}Ar/^{39}Ar$ at 1980 ± 50 ka (Fig. 7; Hoffer et al., 2008). The source of these lavas remains unknown.

Old ages reported from the Ibarra segment

Four $^{40}Ar/^{39}Ar$ ages ranging from 3610 ± 60 to 61 ± 20 ka (Béguelin et al., 2015) have been reported for the Yanaurcu de Piñán volcanic system from the Ibarra segment. Such a very long duration of activity is puzzling, as it has not been observed for any other composite volcano of similar size from the whole Ecuadorian arc. Based on their isotopic ratios (Fig. 8 in Béguelin et al., 2015), it can be

suggested that the Andesitic Old Yanaurcu formation (~3.6 Ma) has a different origin than the younger (<172 ± 20 ka) products of the Yanaurcu de Piñán volcano. These old products could be related to the Late Miocene Pugarán formation, which covers part of the Western Cordillera and is dated at 5.0 ± 2.9 Ma (Boland et al., 2000), or to the Miocene-Pliocene Angochagua formation of the Eastern Cordillera, which is dated between 6.31 ± 0.10 and 3.65 ± 0.07 Ma (Barberi et al., 1988; Boland et al., 2000).

5.3.2. Intermediate stage: 1.4 to 0.6 Ma

During the intermediate construction stage, several new edifices were constructed in the Quito segment and in the southern area of the Ibarra segment (dark to light green fields, Fig. 7). At the end of this stage, new volcanic activity occurred in the Tulcán segment to the north and in the Machachi and Ambato segments to the south, where only a few new structures appeared.

Quito segment

In the Eastern Cordillera, the activity of the **Chacana** caldera (dark green field, 8) is associated with massive lava sequences overlain by voluminous ignimbrite deposits and obsidian flows (Hall and Mothes, 2008c; Beate and Urquizo, 2015). The sequence outcropping on the western caldera flank has been dated between 1350 ± 90 and 1580 ± 70 ka (Bigazzi et al., 2005; Opdyke et al., 2006). To the north, the overlying El Tablón obsidian flow, dated at 810 ± 50 ka (Bigazzi et al., 2005), provides the younger bound for the Chacana caldera formation. Notably, the eastern flank of the oldest Coturco volcano (Fig. 8) seems to be covered by these sequences, further supporting the new K-Ar age of 1959 ± 28 ka obtained here for this volcano (Table 1).

Further north, the **Pambamarca** and **Puntas** volcanoes (Fig. 8) were built on the northwestern and western flanks of the Chacana caldera. The eruptive activity of these andesitic volcanoes occurred while the Chacana caldera was already active, as indicated by our K-Ar ages ranging from 1261 ± 18 to 1374 ± 21 ka for Pambamarca volcano, and from 1132 ± 16 to 1084 ± 17 ka for Puntas volcano

(Table 1). The Pambamarca activity ended with the extrusion of the summit rhyolitic dome complex at 1292 ± 20 ka (20EQ62). We propose that the main stage of the Chacana caldera may be more recent or contemporaneous with Pambamarca and Puntas volcanoes, considering that the Chacana ignimbrite series partially covered these edifices (Hall and Mothes, 2008c). The age of the post-caldera activity at Chacana is defined by the Plaza de Armas lava sequence, located south of the caldera (Figs. 3, 8) and dated at ~726 ka (Pilicita, 2013), which is roughly coeval with the El Tablón obsidian flow west of the caldera (Ta, Fig. 8), dated at 810 ± 50 ka (Bigazzi et al., 2005).

Volcanic activity in the Western Cordillera seems to have first appeared during this stage. In the southern Quito segment, **La Carcacha** volcano (Atacazo-Ninahuilca volcanic complex) was active at ~1300 ka (LC, Fig. 8; Hidalgo, 2006). It was followed to the north by **El Cinto** volcano (Pichincha volcanic complex), dated at 1112 ± 24 ka (Fig. 8; Robin et al., 2010). El Cinto edifice was later intruded by the Ungi dome at 910 ± 7 ka (Robin et al., 2010). Further north, the activity of **Casitagua** volcano built an andesitic main edifice surrounded by several domes between 898 ± 15 and 785 ± 16 ka (Fig. 8; Alvarado et al., 2014; this study). Then, the construction of the **Lower Rucu Pichincha** edifice took place between the Casitagua and El Cinto volcanoes. The lava sequences of this volcano have been dated between ~850 and ~590 ka (Robin et al., 2010; Alvarado et al., 2014) and are thus contemporaneous with the Casitagua volcano.

In the Guayllabamba valley (Inter-Andean Valley), the activity of the **Ilaló** volcano occurred between 1273 ± 20 and 1112 ± 22 ka, forming an edifice composed of andesitic lava sequences (Fig. 8). Then, the emission of voluminous basaltic andesitic lavas at the northern border of the Guayllabamba valley was dated at 1152 ± 30 ka (Pisque Formation, L3, Fig. 8; Alvarado et al., 2014) and 1038 ± 87 ka (pre-Mojanda lavas, L2, Fig. 8; Bablon et al., 2020a). Finally, the activity of the **Pan de Azúcar** volcano in the Sub-Andean zone (Fig. 8) occurred during this stage at 1150 ± 10 ka (Hoffer, 2008).

Extension to the Ibarra and Machachi segments

During this stage, volcanic activity was also present in the Ibarra and Machachi segments (Fig. 8). **Viejo Cayambe** (Fig. 8) is an ancient edifice formed to the northeast of the Chacana and Pambamarca volcanoes in the Eastern Cordillera (Ibarra segment). This edifice, dated between 1108 ± 11 and 1050 ± 5 ka, was formed by andesitic to dacitic lava sequences that culminated in a caldera-forming eruption (Samaniego et al., 2005). Further south, the activity of **Santa Cruz** volcano (Fig. 7) occurred in the Inter-Andean Valley ~40 km south of La Carcacha volcano (Machachi segment). This edifice was formed by andesitic lava series dated at 702 ± 11 ka and several dacitic domes in the summit area (Santamaría et al., 2022). Furthermore, several obsidian pebbles have been identified in the Cosanga river, in the Sub-Andean zone between the Quito and Machachi segments. These fragments are associated with an unknown source located in the Western Cordillera, probably the **Cosanga** or **Bermejo** centers (Mothes and Hall, 2008a). Two fission-track ages suggest that some of these obsidians were emitted during eruptions that ocurred at 670 ± 6 and 290 ± 20 ka (Bellot-Gurlet et al., 2008).

Coeval activity in other segments

Within the Tulcán segment, the lower **Cerro Negro** edifice (Western Cordillera), located on the Colombian border (Fig. 7), was active at 883 ± 19 ka (Telenchana et al., 2017; Bablon, 2018). Further south, in the Latacunga segment, two K-Ar groundmass ages show that the **Sagoatoa** volcano (Fig. 7) was active from at least 826 ± 12 ka to 799 ± 12 ka (Bablon et al., 2019). We note that two unreliable ages at 1850 ± 190 and 1850 ± 240 ka (Lavenu et al., 1995; Opdyke et al., 2006) were obtained from a sequence of basaltic andesite lavas north of **Chinibano** volcano (Fig 7). However, based on erosional features and comparison with other eroded volcanoes, we suggest that this volcano may have been constructed during the intermediate stage of the Ecuadorian arc.

5.3.3. Late stage: from 600 ka

During the late construction stage of the Ecuadorian volcanic arc, a striking increase in the number of active volcanoes can be observed in almost all segments (dark and light blue fields, Fig. 9),

with at least 50 volcanoes active during this period. Although nearly twenty volcanoes remain poorly studied (most of them from the Tulcán and Latacunga segments), Figure 9 suggests that most of the volcanic activity in Ecuador extended over time from the Quito segment both northward and southward. Considering the available data, it is highly plausible that the eruptive history of most of these poorly studied volcanoes occurred during this stage, i.e., the last ~600 ka. As the eruptive histories of the Ibarra, Machachi, Latacunga, Ambato, and Riobamba segments have been presented in detail elsewhere (Bablon et al., 2019, 2020a; Santamaría et al., 2023), we only detail the eruptive history of the Quito segment here.

Quito segment

Volcanic activity in the Quito segment was widespread in both Cordilleras and in the Sub-Andean zone. In the Western Cordillera, the eruptive history of the Rucu Pichincha edifice extended to ~150 ka, including the sector collapse of its western flank (Robin et al., 2010). The westward migration of the vent caused the formation of the Guagua Pichincha edifice as early as ~60 ka, including two sector collapses and the extrusion of several dacitic domes (Robin et al., 2010). The last eruption of Guagua Pichincha took place in 1999-2002 AD. Both edifices form the **Pichincha volcanic complex**. To the north, the highly explosive activity of the **Pululahua dome complex** occurred during the Holocene (Andrade et al., 2021). In the Eastern Cordillera, several obsidian and lava flows were emitted during the resurgent phase of the **Chacana** caldera. The Mullumica and Callejones flows, dated between 200 and 180 ka, are associated with major Plinian eruptions whose pumice fallout deposits, known as the Pifo layers, are key stratigraphic markers of the Guayllabamba basin (Bigazzi et al., 2005; Hall and Mothes, 2008c). To the north of the Chacana caldera, the **Izambi** volcanic series was formed at 370 ± 60 ka (Bigazzi et al., 2005), while the underlying lava sequences probably belong to Chacana (e.g., Aguilera et al., 2007; Hall and Mothes, 2008c). Unlike the adjacent segments, volcanic activity in the Inter-Andean Valley appears to be absent during this stage. However, thick volcaniclastic sequences from both Cordilleras were deposited in the Inter-Andean Valley, resulting in the Guayllabamba and Chiche formations overlying the lacustrine deposits of the San Miguel formation (Villagómez, 2003;

Pacheco et al., 2014). Further west, several rhyolitic eruptions occurred on the western margin of the Cordillera Occidental, to the east of the Chacana caldera (e.g., Cosanga and Bermejo centers; Mothes and Hall, 2008a). Although the eruptive histories of these volcanoes remain poorly documented, radiocarbon determinations and stratigraphic relationships suggest that their activity continued into the Holocene (e.g., El Dorado and Pumayacu centers; Hall and Mothes, 2010). Further west, unpublished $^{40}Ar/^{39}Ar$ ages suggest that the **Sumaco** volcano (Back-Arc) was active between 255 ± 32 and 200 ± 8 ka (Appendix C; M. Fornari pers. com.), with its most recent activity occurring between the 16th and 20th centuries (Salgado et al., 2021).

Holocene volcanism

Among the 78 Quaternary volcanoes identified in our study (Appendix C), 25 were active during the Holocene (Fig. 9). They include Antisana (Hall et al., 2017), Atacazo-Ninahuilca (Hidalgo et al., 2008), Calpi cones (Bablon et al., 2019), Cayambe (Samaniego et al., 1998), Chacana (Hall and Mothes, 2008c), Chachimbiro (Bernard et al., 2014), Chimborazo (Barba et al., 2008), Cotacachi-Cuicocha (Almeida et al., 2023), Cotopaxi (e.g., Hall and Mothes, 2008a), Cubilche (Navarrete et al., 2020), Huañuna (Hall et al., 2017), Iliniza (Santamaría et al., 2022), Imbabura (Le Pennec et al., 2011), Pichincha (Robin et al., 2008), Pululahua (Andrade et al., 2021), Quilotoa (e.g., Di Muro et al., 2008; Mothes and Hall, 2008b), Reventador (e.g., Hall et al., 2004), Sangay (Monzier et al., 1999), Soche (Beate, 1994; Hall and Mothes, 2008b), Sumaco (Salgado et al., 2021), Tungurahua (e.g., Hall et al., 1999; Le Pennec et al., 2013, 2016), and volcanoes on the western side of the Eastern Cordillera El Dorado, Huevos de Chivo, and Pumayacu (Hall and Mothes, 2010). Although there is no clear evidence of significant explosive activity during the Holocene at the Chiles-Cerro Negro volcano (Santamaría et al., 2017), the unrest episode recorded in 2014 AD (Ebmeier et al., 2016) and current fumarolic activity suggest that this volcano is still potentially active. Finally, in the absence of more detailed studies, we do not exclude that other volcanoes may have erupted during the Holocene. For instance, the extrusion of the present-day poorly eroded domes of the Mojanda-Fuya Fuya volcanic complex (e.g., Panecillo

dome; Robin et al., 2009) and Pambamarca volcano (i.e. Herradura dome; this study) could have occurred during the Holocene.

5.4. Relationship between volcanism and tectonics

The ancient NE-SW crustal structures of the Andean Range (black lines, Fig. 10a; Litherland and Aspden, 1992) appear to partially control the alignments of the Ecuadorian arc, especially for frontal volcanoes. Comparable relationships between crustal tectonic structures and the arrangement of volcanoes have also been documented in other Andean volcanic zones (e.g., Acocella et al., 2007; Cembrano and Lara, 2009; González et al., 2009; Salas et al., 2017; Tibaldi et al., 2017) and even worldwide (e.g., Takada, 1994; Tibaldi and Bonali, 2017; Bonali et al., 2018). Indeed, recent evidence suggests that magma storage, differentiation, and mobilization in the Earth's crust are significantly influenced by tectonic controls. Variations in lithology and melt fraction within mush reservoirs create rigidity contrasts that influence the depth of sill intrusion. (e.g., Jackson et al., 2018; van Wyk de Vries and van Wyk de Vries, 2018). Thus, several authors highlighted the arrangement of eruptive centers and/or dykes as a response to regional tectonic stress (e.g., Delaney et al., 1986; Cembrano and Lara, 2009; Sychev et al., 2019; Díaz et al., 2020). Moreover, the distribution of volcanoes and unrest periods also appear to be influenced by local stress regimes and the mechanical properties of the bedrock, which ultimately affect the magma pressure in the conduit (e.g., Gudmundsson, 2006; Gudmundsson and Philipp, 2006; Ebmeier et al., 2016). Consequently, the spatial distribution of volcanoes can result from both deep (i.e., slab dehydration reactions, mantle heterogeneities) and shallow (i.e., tectonics, basement structure) controls. Following the approach of Cembrano and Lara (2009), we discuss below the volcano-tectonic relationship for present-day active and inactive (inherited) crustal structures of the Ecuadorian arc.

Volcanoes over inherited basement structures

In the Western Cordillera, edifices of the Volcanic Front overlie the ancient margin-parallel Pujilí and Toachi thrust-belts sutures, which could serve as passive pathways for magma ascent. These NNE-SSW trending fault systems (black lines, Fig. 10a) separate the Cretaceous oceanic plateau basalts and ophiolites units (e.g., San Juan (K_{Sj}) and Pallatanga (K_{Pa}) Formations) to the East, from the Paleogene to Eocene volcanic and volcanoclastic units (e.g., Macuchi Formation (PcE_M)) to the West (Hughes and Bermúdez, 1997; Hughes and Pilatasig, 2002; Vallejo et al., 2019). The Chachimbiro, Cotacachi, Pichincha, Iliniza, Sagoatoa, and Chimborazo volcanoes from the Western Cordillera are located over the Pujilí-Pallatanga suture zone, whereas Almas Santas and Quilotoa, the westernmost volcanoes of the arc, lie above the Chimbo-Toachi suture zone (Fig. 10a; Hughes and Pilatasig, 2002; Vallejo et al., 2019). The relationship between the basement structures and distribution of volcanism is less obvious in the Eastern Cordillera. However, we note that the eruptive centers of Pambamarca, Puntas, Sincholagua and Cotopaxi on one side, and Cayambe, Chacana, Antisana, and Chalupas on the other side show N-S alignments (Fig. 10a). Although the reverse fault structures of the western margin of the Eastern Cordillera are hidden by a thick Pliocene volcaniclastic cover (e.g. Pisayambo (PL_{Py}) and Angamarca (PL_{An}) Formations), their existence is inferred from the scarce exposures further north in the Chota Valley and in the Pisayambo zone to the south (Litherland et al., 1994; Winkler et al., 2005). These major fault systems separate the metamorphic groups formed during the Triassic anatexis and posterior accretion of the Jurassic para-autochthonous terrains (Litherland et al., 1994; Villagómez et al., 2011; Spikings et al., 2015). For instance, the group composed of Pambamarca, Puntas, Sincholagua and Cotopaxi volcanoes was constructed over the Peltetec suture zone (Litherland et al., 1994; Vallejo et al., 2019). Further west, the Mojanda, Ilaló, Pasochoa, and Rumiñahui alignment might also indicate the presence of inherited basement structures beneath the Inter-Andean Valley. Nonetheless, exposures of the basement of the Inter-Andean valley are scarce, resulting in an incomplete understanding of the suture architecture created by the accretion of the Western Cordillera terrains (Litherland et al., 1994; Hughes and Pilatasig, 2002). Farther east, the Back-Arc volcanoes are built near basement-involved thrust belt faults related to the Napo Uplift, which was formed by the eastward thrusting of the Western Cordillera (Bès de Berc et al., 2005; Gutiérrez et al., 2019). Although several of these structures are still active, their extent and behavior remain poorly documented.

Volcanoes over present-day compressional or trans-pressional tectonics

Although several active fault systems (fs) have been identified in the Ecuadorian Andes (red lines, Fig. 10b; e.g., Alvarado et al., 2016), their relationship to volcanic landforms is not straightforward (Andrade, 2009). For instance, few volcanoes are found near or over the CCPP-fs, the major tectonic structure in Ecuador that connects several trans-pressive and reverse subsystems from the Gulf of Guayaquil (Fig. 1a) to the eastern border of the Eastern Cordillera. The CCPP-fs intersects the Inter-Andean Valley in the Ambato segment and runs through the Calpi cones and the Igualata, Huisla, and Mulmul volcanoes (e.g., Bablon et al., 2019; Baize et al., 2020), but does not coincide with the whole Ambato volcanic cluster. Figure 10b shows that many volcanoes from the arc do not overlie major fault-systems, although their evolution may be influenced by fault kinematics (Tibaldi et al., 2007; Alvarado et al., 2016). For instance, the Billecocha subsystem (B-fs) may have influenced the orientation of the Cotacachi sector collapses as well as their subsequent reconstruction patterns (Jomard et al., 2021; Almeida et al., 2023). Further east, the Alambi subsystem (A-fs) played a key role in the preferential growth patterns of the Imbabura volcano (Andrade et al., 2019). The central part of the arc lies in the interaction zone between the Quito and Latacunga reverse fault systems (QL-fs), which are expressed to the north and south of the segment as parallel strands of folds overlying major west-dipping, blind, *en echelon* thrust faults (Fiorini and Tibaldi, 2012; Alvarado et al., 2014, 2016). Notably, several segments of the Quito-fs are curved around volcanic edifices suggesting that the onset of volcanic activity preceded tectonic activity (Alvarado et al., 2014).

5.5. Relationship between volcanism, the Nazca slab and induced crustal stress

Numerical reconstructions can be used to estimate the present-day bulk volume of volcanic edifices and infer the volume of material accumulated at the end of their construction phases (e.g., Grosse et al., 2013; Germa et al., 2015; Ricci et al., 2015; Bablon et al., 2018, 2020a; Santamaría et al., 2022; Santamaria et al., 2023). A summary of the available volumetric data for Ecuadorian volcanoes,

along with their activity periods, is presented in Appendix D. These data show a first-order correlation between the area (S) covered by each volcanic edifice and the volume (V) of accumulated material, with the relationship $V = 0.42\ S$ (Figure 11). This equation was then used to derive a rough estimate of the cone-building volume for the nine dated stratovolcanoes for which no volumetric data are reported in the literature (i.e., Casitagua, Chachimbiro, Coturco, Ilaló, Pambamarca, Pan de Azúcar, Puntas, Reventador, Yanahurcu de Piñán). Since the eruptive centers with the largest basal areas are located near 0° latitude (Bablon et al., 2020a), the highest volumes of magma were erupted by volcanoes in the Quito and Ibarra segments. Figure 12 shows an exponential increase of the cumulative volume (V) for the whole arc through time (t) according to the relationship $V = 2974e^{-0.003t}$ (R^2=0.977), with a total volume of about 2800 km^3 for the last 2 Myr. The volume of erupted material increased sharply during the late evolutionary stage, from ~500 to ~2760 km^3. The erupted volume (DRE) for the Chalupas, Cuicocha, and Quilotoa calderas were included in this estimate (Crosweller et al., 2012). It must be acknowledged that these data are rough estimates that require further investigations. Accordingly, future studies must take into account several factors, including tephra dispersion, tephra versus lava production, volcanic deposit density variations , numerical reconstruction techniques, and uncertainty in numerical values (e.g., Yamamoto et al., 2018; Bablon et al., 2020a; O'Hara and Karlstrom, 2023; Santamaria et al., 2023). Moreover, the lack of geochronological and stratigraphic data for several volcanoes may affect the accuracy of these estimates. For instance, the Chacana caldera lacks adequate estimates of the volume of material erupted during its long-lived explosive activity, which has been extensively eroded and/or widely dispersed. Whatsoever, Figure 12 provides an interesting overview of the evolution of the Ecuadorian arc, with a strong increase in magmatic productivity coeval with the northward and southward extension of the arc observed during the Late stage since 600 ka.

The spatial distribution of volcanic clusters toward the center of the Ecuadorian arc, together with long-lived volcanism exclusively located within the Quito and Ibarra segments, and with the widest range of incompatible element contents for products of edifices located around 0.5°S (Figure E1; e.g., Ancellin et al., 2017), suggests the highest magma generation rates. The Nazca slab beneath Ecuador has a contorted surface, where the projection of the Grijalva FZ coincides with an inferred slab flexure

at depth (Fig. 1a; Yepes et al., 2016). Bablon et al. (2019) proposed that the apparent southward extension of volcanism from the Ambato segment, above the Grijalva FZ, may have been influenced by changes in the slab geometry, and therefore changes in pressure and temperature conditions, during the last 1 Myr. Additional mechanisms are needed to explain the spreading of volcanism observed since the early stage of the Ecuadorian arc, must be invoked. Since at least ~2.5 Ma, intense volcanism seems to be mainly present in the Quito segment, which lies above the projection of the Carnegie Ridge (Fig. 1a). Recent geochemical signatures highlight that the sub-arc mantle wedge is heterogeneously metasomatized by aqueous fluids and siliceous melts from slab dehydration and partial melting (Ancellin et al., 2017; Narvaez et al., 2018). This evidence may indicate a higher thermal gradient of the sub-arc slab consistent with the position of the Carnegie Ridge. Thus, the thermal regime of the subducting young Nazca crust and the Carnegie Ridge likely favored magma generation since the Early Pleistocene.

The increase in the emission rate of volcanic products, and thus the spread of volcanism described above, may also be related to variations in the crustal stress field, in addition to changes in the magmatic production rate associated with variations in slab geometry and rheology. Indeed, the timing of the increase in the volcanic activity seems to coincide with other regional tectonic events, such as: (1) the cessation of the Late Pliocene WNW–ESE compressional phase registered in the Chota basin (Fig. 2; northern Ecuadorian Andes) prior to the Late Pleistocene, as indicated by the deformed dykes and sills (AFT age: 3.7 ± 1.7 Ma) unconformably overlain by the undeformed volcaniclastic rocks (ZFT age: 0.5 ± 0.2 Ma; Barragán et al., 1996; Winkler et al., 2005); (2) the formation of the Quito-Latacunga microblock during the Pleistocene as a consequence of the latest stage of the North Andean Sliver deformation zone from the Western Cordillera to the east of the Eastern Cordillera, through the creation (or reactivation) and abandonment of tectonic structures over time to accommodate convergent directions (Alvarado et al., 2016); and (3) the Late Pleistocene increase in subsidence and deposition rates reported in the Gulf of Guayaquil (Fig. 1a), recorded by the up to 4 km thick sediment stack, dated by foraminiferal chronobiozones and marine transgression-regressive structures, overlying the thinner Pliocene series (Witt et al., 2006; Witt and Bourgois, 2010; Loayza et al., 2013; Peuzin et al., 2023).

These surface observations of upper crustal dynamics during the Pleistocene may reflect changes at depth, probably related to increased plate coupling at the subduction interface and the presence of the subducting Carnegie Ridge and South American plate (e.g., Margirier et al., 2023).

6. CONCLUSIONS

After three decades of vulcanological research on the Ecuadorian Andean volcanism, the numerous published geochronological data have been compiled, helping to improve knowledge of the eruptive history of Quaternary volcanoes and to define the spatial and temporal evolution of volcanism in the whole arc. The ~250 radioisotope ages included in this geochronological data compilation show that the Ecuadorian arc was constructed in three main stages, with an overall increase in the number of active volcanoes. Based on our dataset, we propose that (1) volcanism began at least 2.5 Ma ago in the central part of the Ecuadorian arc (Quito segment) with the formation of the Coturco volcano and the onset of activity of the Chacana caldera in the Eastern Cordillera. Minor volcanic activity seems to have occurred in the southern Back-Arc (Ambato segment) with the emission of remote scoria cones and lava flows (Hoffer et al., 2008). (2) Volcanic activity extended around the Guayllabamba valley at ~1.4 Ma, as evidenced by products from Cayambe (Samaniego et al., 2005), Pambamarca, Puntas, Casitagua (this study), Pichincha (El Cinto and Rucu Pichincha; Robin et al., 2010), and La Carcacha (Atacazo volcanic complex; Hidalgo, 2006), followed by the construction of the Ilaló volcano and the emission of the Pre-Mojanda (Bablon et al., 2020a) and Pisque lavas (Alvarado et al., 2014) in the Inter-Andean Valley. Toward the end of the intermediate stage (i.e., ~900-600 ka), single edifices appeared in the northern (Cerro Negro; Telenchana et al., 2017; Bablon, 2018), south-central (Santa Cruz; Santamaría et al., 2022), and southern (Sagoatoa; Bablon et al., 2019) zones of the Inter-Andean Valley. (3) A remarkable increase in volcanic activity has occurred since ~600 ka, with at least 50 volcanoes active during this interval. Rather than being homogeneously distributed along the arc, several of these volcanoes were located in areas of a few tens of square kilometers, forming E-W elongated volcanic clusters (e.g., Bablon et al., 2019, 2020a; Santamaría et al., 2023). At least 25 of these volcanoes were active during the Holocene.

The high concentration of volcanoes in the central part of the arc since the beginning of Quaternary volcanism spatially coincides with the inland projection of the Carnegie Ridge. The thermal regime of the subducting young Nazca crust and the Carnegie Ridge thus likely favored magma generation from the Early Pleistocene to the present. Furthermore, the progressive increase of the plate coupling at the subduction interface together with the oblique convergence of the Nazca Plate contributed to the uplift of the Andes and the deformation of the South American plate, with the development of regional crustal fault systems. Therefore, the northward and southward migrations of the arc volcanoes reported here can be explained by the interplay of several factors, including deep control (i.e., slab geometry and age, slab-derived dehydration and melting reactions, mantle heterogeneities), and tectonic reactivation of old structures inherited from the continental crust.

REFERENCES

Acocella, V., Vezzoli, L., Omarini, R., Matteini, M., Mazzuoli, R., 2007. Kinematic variations across Eastern Cordillera at 24°S (Central Andes): Tectonic and magmatic implications. Tectonophysics 434, 81–92. https://doi.org/10.1016/j.tecto.2007.02.001

Aguilera, G., Castilla, W., Nasimba, E., León, E., Calero, B., Pilatasig, L., Gordón, D., 2007. Hoja geológica Cangahua.

Almeida, M., Bablon, M., Andrade, S.D., Hidalgo, S., Quidelleur, X., Vasconez, F.J., Müller, A.V., Lahitte, P., Samaniego, P., 2023. New geological and geochronological constraints on the evolution of the Cotacachi - Cuicocha volcanic complex (Ecuador). Journal of South American Earth Sciences 128, 104489. https://doi.org/10.1016/j.jsames.2023.104489

Alvarado, A., Audin, L., Nocquet, J.M., Jaillard, E., Mothes, P., Jarrín, P., Segovia, M., Rolandone, F., Cisneros, D., 2016. Partitioning of oblique convergence in the Northern Andes subduction zone: Migration history and the present-day boundary of the North Andean Sliver in Ecuador. Tectonics 35, 1048–1065. https://doi.org/10.1002/2016TC004117

Alvarado, A., Audin, L., Nocquet, J.M., Lagreulet, S., Segovia, M., Font, Y., Lamarque, G., Yepes, H., Mothes, P., Rolandone, F., Jarrín, P., Quidelleur, X., 2014. Active tectonics in Quito, Ecuador, assessed by geomorphological studies, GPS data, and crustal seismicity. Tectonics 33, 67–83. https://doi.org/10.1002/2012TC003224

Ancellin, M.-A., Samaniego, P., Vlastélic, I., Nauret, F., Gannoun, A., Hidalgo, S., 2017. Across-arc versus along-arc Sr-Nd-Pb isotope variations in the Ecuadorian volcanic arc. Geochem. Geophys. Geosyst. 18, 1163–1188. https://doi.org/10.1002/2016GC006679

Andrade, S.D., 2009. The influence of active tectonics on the structural development and flank collapse of Ecuadorian arc volcanoes (Ph.D. thesis). Clermont-Ferrand 2, Clermont-Ferrand, France.

Andrade, S.D., Müller, A.V., Vasconez, F.J., Beate, B., Aguilar, J., Santamaría, S., 2021. Pululahua dome complex, Ecuador: eruptive history, total magma output and potential hazards. Journal of South American Earth Sciences 106, 103046. https://doi.org/10.1016/j.jsames.2020.103046

Andrade, S.D., van Wyk de Vries, B., Robin, C., 2019. Imbabura volcano (Ecuador): The influence of dipping-substrata on the structural development of composite volcanoes during strike-slip faulting. Journal of Volcanology and Geothermal Research, Geological data in volcanology: collection, organisation and applications 385, 68–80. https://doi.org/10.1016/j.jvolgeores.2018.11.017

Araujo, S., Valette, B., Potin, B., Ruiz, M., 2021. A preliminary seismic travel time tomography beneath Ecuador from data of the national network. Journal of South American Earth Sciences 111, 103486. https://doi.org/10.1016/j.jsames.2021.103486

Aspden, J.A., Bonilla, W., Duque, P., 1995. The El Oro metamorphic complex, Ecuador: geology and economic mineral deposits, Overseas geology and mineral resources. British Geological Survey, Keyworth, Nottingham.

Aspden, J.A., Harrison, S.H., Rundle, C.C., 1992. New geochronological control for the tectono-magmatic evolution of the metamorphic basement, Cordillera Real and El Oro Province of Ecuador. Journal of South American Earth Sciences 6, 77–96. https://doi.org/10.1016/0895-9811(92)90019-U

Bablon, M., 2018. Reconstruction de l'histoire des volcans de l'arc équatorien : contraintes pour l'évolution chronologique de l'arc andin et pour l'évaluation du risque volcanique (Ph.D. thesis). Université Paris Saclay (COmUE), Orsay, France.

Bablon, M., Quidelleur, X., Samaniego, P., Le Pennec, J.-L., Audin, L., Jomard, H., Baize, S., Liorzou, C., Hidalgo, S., Alvarado, A., 2019. Interactions between volcanism and geodynamics in the southern termination of the Ecuadorian arc. Tectonophysics 751, 54–72. https://doi.org/10.1016/j.tecto.2018.12.010

Bablon, M., Quidelleur, X., Samaniego, P., Le Pennec, J.-L., Lahitte, P., Liorzou, C., Bustillos, J.E., Hidalgo, S., 2018. Eruptive chronology of Tungurahua volcano (Ecuador) revisited based on new K-Ar ages and geomorphological reconstructions. Journal of Volcanology and Geothermal Research 357, 378–398. https://doi.org/10.1016/j.jvolgeores.2018.05.007

Bablon, M., Quidelleur, X., Samaniego, P., Le Pennec, J.-L., Santamaría, S., Liorzou, C., Hidalgo, S., Eschbach, B., 2020a. Volcanic history reconstruction in northern Ecuador: insights for eruptive and erosion rates on the whole Ecuadorian arc. Bull Volcanol 82, 11. https://doi.org/10.1007/s00445-019-1346-1

Bablon, M., Quidelleur, X., Siani, G., Samaniego, P., Le Pennec, J.-L., Nouet, J., Liorzou, C., Santamaría, S., Hidalgo, S., 2020b. Glass shard K-Ar dating of the Chalupas caldera major eruption: Main Pleistocene stratigraphic marker of the Ecuadorian volcanic arc. Quaternary Geochronology 57, 101053. https://doi.org/10.1016/j.quageo.2020.101053

Baby, P., Rivadeneira, M., Barragán, R., Christophoul, F., 2013. Thick-skinned tectonics in the Oriente foreland basin of Ecuador. Geological Society, London, Special Publications 377, 59–76. https://doi.org/10.1144/SP377.1

Baize, S., Audin, L., Alvarado, A., Jomard, H., Bablon, M., Champenois, J., Espin, P., Samaniego, P., Quidelleur, X., Le Pennec, J.-L., 2020. Active Tectonics and Earthquake Geology Along the Pallatanga Fault, Central Andes of Ecuador. Frontiers in Earth Science 8, 193. https://doi.org/10.3389/feart.2020.00193

Ball, P., 2015. Geochemical Analysis of Ecuadorian Back-Arc Lavas (Master's thesis). University of Oxford, Oxford, UK.

Barba, D., Robin, C., Samaniego, P., Eissen, J.-P., 2008. Holocene recurrent explosive activity at Chimborazo volcano (Ecuador). Journal of Volcanology and Geothermal Research, Recent and active volcanism in the Ecuadorian Andes 176, 27–35. https://doi.org/10.1016/j.jvolgeores.2008.05.004

Barberi, F., Coltelli, M., Ferrara, G., Innocenti, F., Navarro, J.M., Santacroce, R., 1988. Plio-quaternary volcanism in Ecuador. Geological Magazine 125, 1–14.

Barragán, R., Baudino, R., Marocco, R., 1996. Geodynamic evolution of the Neogene intermontane Chota basin, Northern Andes of Ecuador. Journal of South American Earth Sciences 9, 309–319. https://doi.org/10.1016/S0895-9811(96)00016-8

Barragan, R., Geist, D., Hall, M., Larson, P., Mark Kurz, 1998. Subduction controls on the compositions of lavas from the Ecuadorian Andes. Earth and Planetary Science Letters 154, 153–166. https://doi.org/10.1016/S0012-821X(97)00141-6

Beate, B., 1994. El Soche: Un volcán activo en la Provincia de Sucumbíos, Ecuador - primeros datos descriptivos, in: Lachowicz, H. (Ed.), . Presented at the Terceras Jornadas en Ciéncias de la Tierra, Facultad de Geologia, Escuela Politécnica Nacional, Quito, Ecuador, pp. 9–10.

Beate, B., 1985. El flujo piroclastico de Chalupas como causante de un desastre natural en el Cuaternario de los Andes Septentrionales del Ecuador, in: Espinosa, T. (Ed.), . Presented at the Primer Simposio Latinoamericano sobre Desastres Naturales, Quito, Ecuador, pp. 21–27.

Beate, B., Inguaggiato, S., Villares, F., Benitez, S., Hidalgo, S., 2010. The Cachiyacu Geothermal Prospect, Chacana Caldera, Ecuador, in: Proceedings World Geothermal Congress. Presented at the World Geothermal Congress, Bali, Indonesia, pp. 1–9.

Beate, B., Urquizo, M., 2015. Geothermal Country Update for Ecuador: 2010-2015, in: Proceedings World Geothermal Congress. pp. 19–24.

Béguelin, P., Chiaradia, M., Beate, B., Spikings, R., 2015. The Yanaurcu volcano (Western Cordillera, Ecuador): A field, petrographic, geochemical, isotopic and geochronological study. Lithos 218–219, 37–53. https://doi.org/10.1016/j.lithos.2015.01.014

Bellot-Gurlet, L., Dorighel, O., Poupeau, G., 2008. Obsidian provenance studies in Colombia and Ecuador: obsidian sources revisited. Journal of Archaeological Science 35, 272–289. https://doi.org/10.1016/j.jas.2007.03.008

Bellver-Baca, M.T., Chiaradia, M., Beate, B., Beguelin, P., Deriaz, B., Mendez-Chazarra, N., Villagómez, D., 2020. Geochemical evolution of the Quaternary Chachimbiro Volcanic Complex (frontal volcanic arc of Ecuador). Lithos 356–357, 105237. https://doi.org/10.1016/j.lithos.2019.105237

Bernard, B., Andrade, D., 2011. Volcanes Cuaternarios del Ecuador Continental. IGEPN Poster Informativo.

Bernard, B., Hidalgo, S., Robin, C., Beate, B., Quijozaca, J., 2014. The 3640–3510 BC rhyodacite eruption of Chachimbiro compound volcano, Ecuador: a violent directed blast produced by a satellite dome. Bull Volcanol 76, 849. https://doi.org/10.1007/s00445-014-0849-z

Bès de Berc, S., Soula, J.C., Baby, P., Souris, M., Christophoul, F., Rosero, J., 2005. Geomorphic evidence of active deformation and uplift in a modern continental wedge-top–foredeep transition: Example of the eastern Ecuadorian Andes. Tectonophysics, Andean Geodynamics: 399, 351–380. https://doi.org/10.1016/j.tecto.2004.12.030

Bigazzi, G., Coltelli, M., Hadler, N.J.C., Araya, A.M.O., Oddone, M., Salazar, E., 1992. Obsidian-bearing lava flows and pre-Columbian artifacts from the Ecuadorian Andes: First new multidisciplinary data. Journal of South American Earth Sciences 6, 21–32. https://doi.org/10.1016/0895-9811(92)90014-P

Bigazzi, G., Hadler Neto, J.C., Iunes, P.J., Osório Araya, A.M., 2005. Fission-track dating of South American natural glasses: an overview. Radiation Measurements, Proceedings of the 2nd Latin American Symposium on Nuclear Tracks 39, 585–594. https://doi.org/10.1016/j.radmeas.2004.09.006

Boland, M., Ibadango, E., Pilatasig, L.F., McCourt, W., Aspden, J.A., Hughen, R., Beate, B., 2000. Geology of the Cordillera Occidental of Ecuador between 0°00’ and 1°00’N (No. 10), Proyecto de Desarrollo Minero y Control Ambiental. Cogidem - British Geological Survey, Quito.

Bonali, F.L., Tibaldi, A., Pasquaré Mariotto, F., Russo, E., 2018. Interplay between inherited rift faults and strike-slip structures: Insights from analogue models and field data from Iceland. Global and Planetary Change, From the deep Earth to the surface 171, 88–109. https://doi.org/10.1016/j.gloplacha.2018.03.009

Bourdon, E., Eissen, J.-P., Gutscher, M.-A., Monzier, M., Hall, M.L., Cotten, J., 2003. Magmatic response to early aseismic ridge subduction: the Ecuadorian margin case (South America). Earth and Planetary Science Letters 205, 123–138. https://doi.org/10.1016/S0012-821X(02)01024-5

Bryant, J.A., Yogodzinski, G.M., Hall, M.L., Lewicki, J.L., Bailey, D.G., 2006. Geochemical Constraints on the Origin of Volcanic Rocks from the Andean Northern Volcanic Zone, Ecuador. Journal of Petrology 47, 1147–1175. https://doi.org/10.1093/petrology/egl006

Cembrano, J., Lara, L., 2009. The link between volcanism and tectonics in the southern volcanic zone of the Chilean Andes: A review. Tectonophysics, Understanding stress and deformation in active volcanoes 471, 96–113. https://doi.org/10.1016/j.tecto.2009.02.038

Chiaradia, M., Bellver-Baca, M.T., Valverde, V., Spikings, R., 2021. Geochemical and isotopic variations in a frontal arc volcanic cluster (Chachimbiro-Pulumbura-Pilavo-Yanaurcu, Ecuador). Chemical Geology 574, 120240. https://doi.org/10.1016/j.chemgeo.2021.120240

Chiaradia, M., Müntener, O., Beate, B., 2020. Effects of aseismic ridge subduction on the geochemistry of frontal arc magmas. Earth and Planetary Science Letters 531, 115984. https://doi.org/10.1016/j.epsl.2019.115984

Chiaradia, M., Müntener, O., Beate, B., 2014. Quaternary Sanukitoid-like Andesites Generated by Intracrustal Processes (Chacana Caldera Complex, Ecuador): Implications for Archean Sanukitoids. Journal of Petrology 55, 769–802. https://doi.org/10.1093/petrology/egu006

Chiaradia, M., Müntener, O., Beate, B., Fontignie, D., 2009. Adakite-like volcanism of Ecuador: lower crust magmatic evolution and recycling. Contrib Mineral Petrol 158, 563–588. https://doi.org/10.1007/s00410-009-0397-2

Clapperton, C.M., 1990. Glacial and volcanic geomorphology of the Chimborazo-Carihuairazo Massif, Ecuadorian Andes. Earth and Environmental Science Transactions of The Royal Society of Edinburgh 81, 91–116. https://doi.org/10.1017/S0263593300005174

Cotten, J., Le Dez, A., Bau, M., Caroff, M., Maury, R.C., Dulski, P., Fourcade, S., Bohn, M., Brousse, R., 1995. Origin of anomalous rare-earth element and yttrium enrichments in subaerially exposed basalts: Evidence from French Polynesia. Chemical Geology 119, 115–138. https://doi.org/10.1016/0009-2541(94)00102-E

Crosweller, H.S., Arora, B., Brown, S.K., Cottrell, E., Deligne, N.I., Guerrero, N.O., Hobbs, L., Kiyosugi, K., Loughlin, S.C., Lowndes, J., Nayembil, M., Siebert, L., Sparks, R.S.J., Takarada, S., Venzke, E., 2012. Global database on large magnitude explosive volcanic eruptions (LaMEVE). Journal of Applied Volcanology 1, 4. https://doi.org/10.1186/2191-5040-1-4

Delaney, P.T., Pollard, D.D., Ziony, J.I., McKee, E.H., 1986. Field relations between dikes and joints: Emplacement processes and paleostress analysis. Journal of Geophysical Research: Solid Earth 91, 4920–4938. https://doi.org/10.1029/JB091iB05p04920

DeMets, C., Gordon, R.G., Argus, D.F., 2010. Geologically current plate motions. Geophysical Journal International 181, 1–80. https://doi.org/10.1111/j.1365-246X.2009.04491.x

Di Muro, A., Rosi, M., Aguilera, E., Barbieri, R., Massa, G., Mundula, F., Pieri, F., 2008. Transport and sedimentation dynamics of transitional explosive eruption columns: The example of the 800 BP Quilotoa plinian eruption (Ecuador). Journal of Volcanology and Geothermal Research 174, 307–324. https://doi.org/10.1016/j.jvolgeores.2008.03.002

Díaz, D., Zúñiga, F., Castruccio, A., 2020. The interaction between active crustal faults and volcanism: A case study of the Liquiñe-Ofqui Fault Zone and Osorno volcano, Southern Andes, using magnetotellurics. Journal of Volcanology and Geothermal Research 393, 106806. https://doi.org/10.1016/j.jvolgeores.2020.106806

Dibacto, S., Lahitte, P., Karátson, D., Hencz, M., Szakács, A., Biró, T., Kovács, I., Veres, D., 2020. Growth and erosion rates of the East Carpathians volcanoes constrained by numerical models: Tectonic and climatic implications. Geomorphology 368, 107352. https://doi.org/10.1016/j.geomorph.2020.107352

Ebmeier, S.K., Elliott, J.R., Nocquet, J.-M., Biggs, J., Mothes, P., Jarrín, P., Yépez, M., Aguaiza, S., Lundgren, P., Samsonov, S.V., 2016. Shallow earthquake inhibits unrest near Chiles–Cerro Negro volcanoes, Ecuador–Colombian border. Earth and Planetary Science Letters 450, 283–291. https://doi.org/10.1016/j.epsl.2016.06.046

Egüez, A., Gaona, M., Albán, A., 2017. Mapa Geológico de la República del Ecuador.

Fiorini, E., Tibaldi, A., 2012. Quaternary tectonics in the central Interandean Valley, Ecuador: Fault-propagation folds, transfer faults and the Cotopaxi Volcano. Global and Planetary Change, Coupled deep Earth and surface processes in System Earth: monitoring, reconstruction and process modeling 90–91, 87–103. https://doi.org/10.1016/j.gloplacha.2011.06.002

Fleck, R.J., Sutter, J.F., Elliot, D.H., 1977. Interpretation of discordant 40Ar/39Ar age-spectra of mesozoic tholeiites from antarctica. Geochimica et Cosmochimica Acta 41, 15–32. https://doi.org/10.1016/0016-7037(77)90184-3

Garrison, J., Davidson, J., Reid, M., Turner, S., 2006. Source versus differentiation controls on U-series disequilibria: Insights from Cotopaxi Volcano, Ecuador. Earth and Planetary Science Letters 244, 548–565. https://doi.org/10.1016/j.epsl.2006.02.013

Garrison, J.M., Sims, K.W.W., Yogodzinski, G.M., Escobar, R.D., Scott, S., Mothes, P., Hall, M.L., Ramon, P., 2017. Shallow-level differentiation of phonolitic lavas from Sumaco Volcano, Ecuador. Contrib Mineral Petrol 173, 6. https://doi.org/10.1007/s00410-017-1431-4

Geotérmica Italiana, 1989. Mitigación del riesgo volcánico en el área metropolitana de Quito (Informe final No. 2). INEMIN, DGCS, Pisa, Italy.

Germa, A., Lahitte, P., Quidelleur, X., 2015. Construction and destruction of Mont Pelée volcano: Volumes and rates constrained from a geomorphological model of evolution. Journal of Geophysical Research: Earth Surface 120, 1206–1226. https://doi.org/10.1002/2014JF003355

Gillot, P.-Y., Cornette, Y., Max, N., Floris, B., 1992. Two reference materials, Trachytes MDO-G and ISH-G, for Argon Dating (K-Ar and 40Ar/39Ar) of Pleistocene and Holocene rocks. Geostandards Newsletter 16, 55–60. https://doi.org/10.1111/j.1751-908X.1992.tb00487.x

Gillot, P.Y., Hildenbrand, A., Lefèvre, J.C., Albore-Livadie, C., 2006. The K/Ar dating method: principle, analytical techniques, and application to Holocene volcanic eruptions in Southern Italy. Acta Vulcanologica 18, 55–66.

González, G., Cembrano, J., Aron, F., Veloso, E.E., Shyu, J.B.H., 2009. Coeval compressional deformation and volcanism in the central Andes, case studies from northern Chile (23°S–24°S). Tectonics 28. https://doi.org/10.1029/2009TC002538

Grosse, P., Euillades, P.A., Euillades, L.D., van Wyk de Vries, B., 2013. A global database of composite volcano morphometry. Bull Volcanol 76, 784. https://doi.org/10.1007/s00445-013-0784-4

Grosse, P., Ochi Ramacciotti, M.L., Escalante Fochi, F., Guzmán, S., Orihashi, Y., Sumino, H., 2020. Geomorphology, morphometry, spatial distribution and ages of mafic monogenetic volcanoes of the Peinado and Incahuasi fields, southernmost Central Volcanic Zone of the Andes. Journal of Volcanology and Geothermal Research 401, 106966. https://doi.org/10.1016/j.jvolgeores.2020.106966

Grosse, P., Orihashi, Y., Guzmán, S.R., Sumino, H., Nagao, K., 2018. Eruptive history of Incahuasi, Falso Azufre and El Cóndor Quaternary composite volcanoes, southern Central Andes. Bull Volcanol 80, 1–26. https://doi.org/10.1007/s00445-018-1221-5

Gudmundsson, A., 2006. How local stresses control magma-chamber ruptures, dyke injections, and eruptions in composite volcanoes. Earth-Science Reviews 79, 1–31. https://doi.org/10.1016/j.earscirev.2006.06.006

Gudmundsson, A., Philipp, S.L., 2006. How local stress fields prevent volcanic eruptions. Journal of Volcanology and Geothermal Research 158, 257–268. https://doi.org/10.1016/j.jvolgeores.2006.06.005

Gutiérrez, E.G., Horton, B.K., Vallejo, C., Jackson, L.J., George, S.W.M., 2019. Chapter 9 - Provenance and geochronological insights into Late Cretaceous-Cenozoic foreland basin development in the Subandean Zone and Oriente Basin of Ecuador, in: Horton, B.K., Folguera, A. (Eds.), Andean Tectonics. Elsevier, pp. 237–268. https://doi.org/10.1016/B978-0-12-816009-1.00011-3

Gutscher, M.-A., Malavieille, J., Lallemand, S., Collot, J.-Y., 1999. Tectonic segmentation of the North Andean margin: impact of the Carnegie Ridge collision. Earth and Planetary Science Letters 168, 255–270. https://doi.org/10.1016/S0012-821X(99)00060-6

Hall, M., Ramón, P., Mothes, P., LePennec, J.L., García, A., Samaniego, P., Yepes, H., 2004. Volcanic eruptions with little warning: the case of Volcán Reventador's Surprise November 3, 2002 Eruption, Ecuador. Revista geológica de Chile 31, 349–358. https://doi.org/10.4067/S0716-02082004000200010

Hall, M.L., 1977. El volcanismo en el Ecuador. Instituto Panamericano de Geografía e Historia, Quito.

Hall, M.L., Beate, B., 1991. El volcanismo plio cuaternario en los Andes del Ecuador, in: El paisaje volcánico de la sierra ecuatoriana: geomorfología, fenómenos volcánicos y recursos asociados, Estudios de Geografia. Corporación Editora Nacional, Quito, pp. 5–17.

Hall, M.L., Mothes, P., 2010. New active rhyolitic eruption centers - Eastern foot of the Ecuadorian Andes, in: Abstracts Volume. Presented at the Cities on Volcanoes 6th, Tenerife, Spain, p. 44.

Hall, M.L., Mothes, P., 2008a. The rhyolitic–andesitic eruptive history of Cotopaxi volcano, Ecuador. Bull Volcanol 70, 675–702. https://doi.org/10.1007/s00445-007-0161-2

Hall, M.L., Mothes, P., 2008b. Volcanic impediments in the progressive development of pre-Columbian civilizations in the Ecuadorian Andes. Journal of Volcanology and Geothermal Research, Volcanoes and Human History 176, 344–355. https://doi.org/10.1016/j.jvolgeores.2008.01.039

Hall, M.L., Mothes, P.A., 2008c. The Chacana caldera complex in Ecuador, in: Volume 3: Collapse Calderas Workshop. Presented at the IOP Conference Series: Earth and Environmental Science (EES), IOP Publishing, Querétaro, Mexico. https://doi.org/10.1088/1755-1307/3/1/012004

Hall, M.L., Mothes, P.A., 1997. El origen y la edad de la cangahua superior, valle de Tumbaco (Ecuador). Presented at the Suelos volcánicos endurecidos (Quito, diciembre 1996), pp. 19–28.

Hall, M.L., Mothes, P.A., Samaniego, P., Militzer, A., Beate, B., Ramón, P., Robin, C., 2017. Antisana volcano: A representative andesitic volcano of the eastern cordillera of Ecuador: Petrography, chemistry, tephra and glacial stratigraphy. Journal of South American Earth Sciences 73, 50–64. https://doi.org/10.1016/j.jsames.2016.11.005

Hall, M.L., Robin, C., Beate, B., Mothes, P., Monzier, M., 1999. Tungurahua Volcano, Ecuador: structure, eruptive history and hazards. Journal of Volcanology and Geothermal Research 91, 1–21. https://doi.org/10.1016/S0377-0273(99)00047-5

Hall, M.L., Samaniego, P., Le Pennec, J.L., Johnson, J.B., 2008. Ecuadorian Andes volcanism: A review of Late Pliocene to present activity. Journal of Volcanology and Geothermal Research, Recent and active volcanism in the Ecuadorian Andes 176, 1–6. https://doi.org/10.1016/j.jvolgeores.2008.06.012

Hall, M.L., Wood, C.A., 1985. Volcano-tectonic segmentation of the northern Andes. Geology 13, 203–207. https://doi.org/10.1130/0091-7613(1985)13<203:VSOTNA>2.0.CO;2

Hammersley, L.C., 2003. Isotopic evidence for the relative roles of fractional crystallization, crustal assimilation and magma supply in the generation of large volume rhyolitic eruptions (Ph.D. thesis). University of California, Berkeley, CA.

Hidalgo, S., 2006. Les intéractions entre magmas calco-alcalins “classiques” et adakitiques: exemple du complexe volcanique Atacazo-Ninahuilca (Equateur) (Ph.D. thesis). Université Blaise Pascal - Clermont-Ferrand II, Clermont-Ferrand, France.

Hidalgo, S., Gerbe, M.C., Martin, H., Samaniego, P., Bourdon, E., 2012. Role of crustal and slab components in the Northern Volcanic Zone of the Andes (Ecuador) constrained by Sr–Nd–O isotopes. Lithos 132–133, 180–192. https://doi.org/10.1016/j.lithos.2011.11.019

Hidalgo, S., Monzier, M., Almeida, E., Chazot, G., Eissen, J.-P., van der Plicht, J., Hall, M.L., 2008. Late Pleistocene and Holocene activity of the Atacazo–Ninahuilca Volcanic Complex (Ecuador). Journal of Volcanology and Geothermal Research, Recent and active volcanism in the Ecuadorian Andes 176, 16–26. https://doi.org/10.1016/j.jvolgeores.2008.05.017

Hildenbrand, A., Marques, F.O., Catalão, J., 2018. Large-scale mass wasting on small volcanic islands revealed by the study of Flores Island (Azores). Scientific Reports 8, 13898. https://doi.org/10.1038/s41598-018-32253-0

Hoffer, G., 2008. Fusion partielle d’un manteau métasomatisé par un liquide adakitique : approches géochimique et expérimentale de la genèse et de l’évolution des magmas de l’arrière-arc équatorien (Ph.D. thesis). Université Blaise Pascal - Clermont-Ferrand II, Clermont-Ferrand, France.

Hoffer, G., Eissen, J.-P., Beate, B., Bourdon, E., Fornari, M., Cotten, J., 2008. Geochemical and petrological constraints on rear-arc magma genesis processes in Ecuador: The Puyo cones and Mera lavas volcanic formations. Journal of Volcanology and Geothermal Research, Recent and active volcanism in the Ecuadorian Andes 176, 107–118. https://doi.org/10.1016/j.jvolgeores.2008.05.023

Hughes, R.A., Bermúdez, R., 1997. Geology of the Cordillera Occidental of Ecuador between 0°00' and 1°00'S (No. 4), Proyecto de Desarrollo Minero y Control Ambiental. Cogidem - Brithis Geological Survey, Quito.

Hughes, R.A., Pilatasig, L.F., 2002. Cretaceous and Tertiary terrane accretion in the Cordillera Occidental of the Andes of Ecuador. Tectonophysics, Andean Geodynamics ISAG 4 345, 29–48. https://doi.org/10.1016/S0040-1951(01)00205-0

Ibanez-Mejia, M., Ruiz, J., Valencia, V.A., Cardona, A., Gehrels, G.E., Mora, A.R., 2011. The Putumayo Orogen of Amazonia and its implications for Rodinia reconstructions: New U–Pb geochronological insights into the Proterozoic tectonic evolution of northwestern South America. Precambrian Research 191, 58–77. https://doi.org/10.1016/j.precamres.2011.09.005

Jackson, M.D., Blundy, J., Sparks, R.S.J., 2018. Chemical differentiation, cold storage and remobilization of magma in the Earth's crust. Nature 564, 405–409. https://doi.org/10.1038/s41586-018-0746-2

Jaillard, E., 2022. Late Cretaceous-Paleogene orogenic build-up of the Ecuadorian Andes: Review and discussion. Earth-Science Reviews 230, 104033. https://doi.org/10.1016/j.earscirev.2022.104033

Jaillard, E., Ordoñez, M., Suárez, J., Toro, J., Iza, D., Lugo, W., 2004. Stratigraphy of the late Cretaceous–Paleogene deposits of the cordillera occidental of central ecuador: geodynamic implications. Journal of South American Earth Sciences 17, 49–58. https://doi.org/10.1016/j.jsames.2004.05.003

Jarrin, P., Nocquet, J.-M., Rolandone, F., Audin, L., Mora-Páez, H., Alvarado, A., Mothes, P., Audemard, F., Villegas-Lanza, J.C., Cisneros, D., 2023. Continental block motion in the Northern Andes from GPS measurements. Geophysical Journal International 235, 1434–1464. https://doi.org/10.1093/gji/ggad294

Jomard, H., Saqui, D., Baize, S., Alvarado, A., Bernard, B., Audin, L., Hidalgo, S., Pacheco, D., Ruiz, M., Segovia, M., 2021. Interactions between active tectonics and gravitational deformation along the Billecocha fault system (Northern Ecuador): Insights from morphological and paleoseismological investigations. Journal of South American Earth Sciences 111, 103406. https://doi.org/10.1016/j.jsames.2021.103406

Koch, C.D., Delph, J., Beck, S.L., Lynner, C., Ruiz, M., Hernandez, S., Samaniego, P., Meltzer, A., Mothes, P., Hidalgo, S., 2021. Crustal thickness and magma storage beneath the Ecuadorian arc. Journal of South American Earth Sciences 110, 103331. https://doi.org/10.1016/j.jsames.2021.103331

Lavenu, A., Winter, T., Dávila, F., 1995. A Pliocene–Quaternary compressional basin in the Interandean Depression, Central Ecuador. Geophysical Journal International 121, 279–300. https://doi.org/10.1111/j.1365-246X.1995.tb03527.x

Le Pennec, J.-L., de Saulieu, G., Samaniego, P., Jaya, D., Gailler, L., 2013. A Devastating Plinian Eruption at Tungurahua Volcano Reveals Formative Occupation at ~1100 cal BC in Central Ecuador. Radiocarbon 55, 1199–1214. https://doi.org/10.1017/S0033822200048116

Le Pennec, J.-L., Ramón, P., Robin, C., Almeida, E., 2016. Combining historical and 14C data to assess pyroclastic density current hazards in Baños city near Tungurahua volcano (Ecuador). Quaternary International, Volcanic Activity and Human Society 394, 98–114. https://doi.org/10.1016/j.quaint.2015.06.052

Le Pennec, J.L., Ruiz, A.G., Eissen, J.P., Hall, M.L., Fornari, M., 2011. Identifying potentially active volcanoes in the Andes: Radiometric evidence for late Pleistocene-early Holocene eruptions at Volcán Imbabura, Ecuador. Journal of Volcanology and Geothermal Research 206, 121–135. https://doi.org/10.1016/j.jvolgeores.2011.06.002

Litherland, M., Aspden, J.A., 1992. Terrane-boundary reactivation: A control on the evolution of the Northern Andes. Journal of South American Earth Sciences 5, 71–76. https://doi.org/10.1016/0895-9811(92)90060-C

Litherland, M., Aspden, J.A., Jemielita, R.A., 1994. The metamorphic belts of Ecuador, Overseas Memoir Institute of Geological Sciences. British Geological Survey, Keyworth, Nottingham.

Loayza, T.G., Proust, J.-N., Michaud, F., Collot, J.-Y., 2013. Evolution Pléistocène du Système de canyons du Golfe de Guayaquil (Equateur): Contrôles paléo-climatiques et tectoniques. Presented at the 14e Congrès Français de Sédimentologie, Paris, Francia.

Lonsdale, P., 2005. Creation of the Cocos and Nazca plates by fission of the Farallon plate. Tectonophysics 404, 237–264. https://doi.org/10.1016/j.tecto.2005.05.011

Margirier, A., Strecker, M.R., Reiners, P.W., Thomson, S.N., Casado, I., George, S.W.M., Alvarado, A., 2023. Late Miocene Exhumation of the Western Cordillera, Ecuador, Driven by Increased Coupling Between the Subducting Carnegie Ridge and the South American Continent. Tectonics 42, e2022TC007344. https://doi.org/10.1029/2022TC007344

Meschede, M., Barckhausen, U., 2000. Plate Tectonic Evolution of the Cocos-Nazca Spreading Center. Proc. ODP, Sci. Results, Fluid, Mass, and Thermal Fluxes in the Pacific Margin of Costa Rica 170, 1–10. https://doi.org/doi:10.2973/odp.proc.sr.170.009.2000

Monzier, M., Robin, C., Samaniego, P., Hall, M.L., Cotten, J., Mothes, P., Arnaud, N., 1999. Sangay volcano, Ecuador: structural development, present activity and petrology. Journal of Volcanology and Geothermal Research 90, 49–79. https://doi.org/10.1016/S0377-0273(99)00021-9

Mothes, P.A., Hall, M.L., 2008a. Rhyolitic calderas and centers clustered within the active andesitic belt of Ecuador's Eastern Cordillera, in: Volume 3: Collapse Calderas Workshop. Presented at the IOP Conference Series: Earth and Environmental Science, IOP Publishing, Querétaro, Mexico, p. 012007. https://doi.org/10.1088/1755-1307/3/1/012007

Mothes, P.A., Hall, M.L., 2008b. The plinian fallout associated with Quilotoa's 800 yr BP eruption, Ecuadorian Andes. Journal of Volcanology and Geothermal Research, Recent and active volcanism in the Ecuadorian Andes 176, 56–69. https://doi.org/10.1016/j.jvolgeores.2008.05.018

Narvaez, D.F., Rose-Koga, E.F., Samaniego, P., Koga, K.T., Hidalgo, S., 2018. Constraining magma sources using primitive olivine-hosted melt inclusions from Puñalica and Sangay volcanoes (Ecuador). Contrib Mineral Petrol 173, 1–25. https://doi.org/10.1007/s00410-018-1508-8

Navarrete, W.F., Le Pennec, J.L., Solano, S., Liorzou, C., Ruiz, G.A., 2020. A first reconstruction of the evolution of Cubilche Volcanic Complex, Imbabura Province, Ecuador. Journal of Volcanology and Geothermal Research 406, 107023. https://doi.org/10.1016/j.jvolgeores.2020.107023

Nocquet, J.-M., Villegas-Lanza, J.C., Chlieh, M., Mothes, P.A., Rolandone, F., Jarrin, P., Cisneros, D., Alvarado, A., Audin, L., Bondoux, F., Martin, X., Font, Y., Régnier, M., Vallée, M., Tran, T., Beauval, C., Mendoza, J.M.M., Martinez, W., Tavera, H., Yepes, H., 2014. Motion of continental slivers and

creeping subduction in the northern Andes. Nature Geoscience 7, 287–291. https://doi.org/10.1038/ngeo2099

O'Connor, J.M., Stoffers, P., Wijbrans, Jan.R., Worthington, T.J., 2007. Migration of widespread long-lived volcanism across the Galápagos Volcanic Province: Evidence for a broad hotspot melting anomaly? Earth and Planetary Science Letters 263, 339–354. https://doi.org/10.1016/j.epsl.2007.09.007

O'Hara, D., Karlstrom, L., 2023. The arc-scale spatial distribution of volcano erosion implies coupled magmatism and regional climate in the Cascades arc, United States. Frontiers in Earth Science 11.

Opdyke, N.D., Hall, M., Mejia, V., Huang, K., Foster, D.A., 2006. Time-averaged field at the equator: Results from Ecuador. Geochemistry, Geophysics, Geosystems 7. https://doi.org/10.1029/2005GC001221

Pacheco, D., 2013. Estudio Geológico de las formaciones Cuaternarias en la zona San Antonio de Pichincha - Pomasqui (Engineer memoir). Escuela Politécnica Nacional, Quito, Ecuador.

Pacheco, D.A., Andrade, D., Alvarado, A., 2014. Estratigrafía de la Cuenca San Antonio de Pichincha. Revista Politécnica 33.

Papale, P., Rosi, M., 1993. A case of no-wind plinian fallout at Pululagua caldera (Ecuador): implications for models of clast dispersal. Bull Volcanol 55, 523–535. https://doi.org/10.1007/BF00304594

Peccerillo, A., Taylor, S.R., 1976. Geochemistry of eocene calc-alkaline volcanic rocks from the Kastamonu area, Northern Turkey. Contr. Mineral. and Petrol. 58, 63–81. https://doi.org/10.1007/BF00384745

Peuzin, A., Saillard, M., Espurt, N., Michaud, F., Bulois, C., Praeg, D., Régnier, M., Calderon, Y., 2023. Gravity-driven large-scale deformation system in the Tumbes-Guayaquil forearc basin, Northern Andes (Northern Peru-Southern Ecuador). Journal of Structural Geology 173, 104909. https://doi.org/10.1016/j.jsg.2023.104909

Pilicita, B.F., 2013. Estudio de fuentes termales, fallas geológicas, descarga de calor en la Caldera de Chacana y el aprovechamiento actual del recurso geotérmico (Engineer memoir). Escuela Politécnica Nacional, Quito, Ecuador.

Portner, D.E., Rodríguez, E.E., Beck, S., Zandt, G., Scire, A., Rocha, M.P., Bianchi, M.B., Ruiz, M., França, G.S., Condori, C., Alvarado, P., 2020. Detailed Structure of the Subducted Nazca Slab into the Lower Mantle Derived From Continent-Scale Teleseismic P Wave Tomography. Journal of Geophysical Research: Solid Earth 125, e2019JB017884. https://doi.org/10.1029/2019JB017884

Quidelleur, X., Gillot, P.-Y., Carlut, J., Courtillot, V., 1999. Link between excursions and paleointensity inferred from abnormal field directions recorded at La Palma around 600 ka. Earth and Planetary Science Letters 168, 233–242. https://doi.org/10.1016/S0012-821X(99)00061-8

Quidelleur, X., Gillot, P.-Y., Soler, V., Lefèvre, J.-C., 2001. K/Ar dating extended into the last millennium: Application to the youngest effusive episode of the Teide Volcano (Spain). Geophysical Research Letters 28, 3067–3070. https://doi.org/10.1029/2000GL012821

Quidelleur, X., Michon, L., Famin, V., Geffray, M.-C., Danišík, M., Gardiner, N., Rusquet, A., Zakaria, M.G., 2021. Holocene volcanic activity in Anjouan Island (Comoros archipelago) revealed by new

Cassignol-Gillot groundmass K–Ar and 14C ages. Quaternary Geochronology 101236. https://doi.org/10.1016/j.quageo.2021.101236

Raczek, I., Stoll, B., Hofmann, A.W., Peter Jochum, K., 2001. High-Precision Trace Element Data for the USGS Reference Materials BCR-1, BCR-2, BHVO-1, BHVO-2, AGV-1, AGV-2, DTS-1, DTS-2, GSP-1 and GSP-2 by ID-TIMS and MIC-SSMS. Geostandards Newsletter 25, 77–86. https://doi.org/10.1111/j.1751-908X.2001.tb00789.x

Ramon, P., Vallejo, S., Mothes, P., Andrade, D., Vásconez, F., Yepes, H., Hidalgo, S., Santamaría, S., 2021. Instituto Geofísico – Escuela Politécnica Nacional, the Ecuadorian Seismology and Volcanology Service. Volcanica 4, 93–112. https://doi.org/10.30909/vol.04.S1.93112

Ricci, J., Lahitte, P., Quidelleur, X., 2015. Construction and destruction rates of volcanoes within tropical environment: Examples from the Basse-Terre Island (Guadeloupe, Lesser Antilles). Geomorphology 228, 597–607. https://doi.org/10.1016/j.geomorph.2014.10.002

Robin, C., Eissen, J.-P., Samaniego, P., Martin, H., Hall, M., Cotten, J., 2009. Evolution of the late Pleistocene Mojanda–Fuya Fuya volcanic complex (Ecuador), by progressive adakitic involvement in mantle magma sources. Bull Volcanol 71, 233. https://doi.org/10.1007/s00445-008-0219-9

Robin, C., Samaniego, P., Le Pennec, J.-L., Fornari, M., Mothes, P., van der Plicht, J., 2010. New radiometric and petrological constraints on the evolution of the Pichincha volcanic complex (Ecuador). Bull Volcanol 72, 1109–1129. https://doi.org/10.1007/s00445-010-0389-0

Robin, C., Samaniego, P., Le Pennec, J.-L., Mothes, P., van der Plicht, J., 2008. Late Holocene phases of dome growth and Plinian activity at Guagua Pichincha volcano (Ecuador). Journal of Volcanology and Geothermal Research, Recent and active volcanism in the Ecuadorian Andes 176, 7–15. https://doi.org/10.1016/j.jvolgeores.2007.10.008

Salas, P.A., Rabbia, O.M., Hernández, L.B., Ruprecht, P., 2017. Mafic monogenetic vents at the Descabezado Grande volcanic field (35.5°S–70.8°W): the northernmost evidence of regional primitive volcanism in the Southern Volcanic Zone of Chile. Int J Earth Sci (Geol Rundsch) 106, 1107–1121. https://doi.org/10.1007/s00531-016-1357-5

Salgado, J.A., Mothes, P.A., Córdova, M.D., 2021. New observations on the recent eruptive activity of Sumaco Volcano (Ecuador), based on geochronology, stratigraphy and petrography. Journal of South American Earth Sciences 103568. https://doi.org/10.1016/j.jsames.2021.103568

Samaniego, P., Martin, H., Monzier, M., Robin, C., Fornari, M., Eissen, J.-P., Cotten, J., 2005. Temporal Evolution of Magmatism in the Northern Volcanic Zone of the Andes: The Geology and Petrology of Cayambe Volcanic Complex (Ecuador). Journal of Petrology 46, 2225–2252. https://doi.org/10.1093/petrology/egi053

Samaniego, P., Martin, H., Robin, C., Monzier, M., 2002. Transition from calc-alkalic to adakitic magmatism at Cayambe volcano, Ecuador: Insights into slab melts and mantle wedge interactions. Geology 30, 967. https://doi.org/10.1130/0091-7613(2002)030<0967:TFCATA>2.0.CO;2

Samaniego, P., Monzier, M., Robin, C., Hall, M.L., 1998. Late Holocene eruptive activity at Nevado Cayambe Volcano, Ecuador. Bull Volcanol 59, 451–459. https://doi.org/10.1007/s004450050203

Samaniego, P., Ordóñez, J., Bablon, M., Hall, M.L., Quidelleur, X., Lahitte, P., Santamaria, S., Liorzou, C., 2022. The eruptive chronology of the Carihuairazo volcano (Ecuador): Recurrent sector collapses

of a Middle Pleistocene stratovolcano of the northern andes. Journal of South American Earth Sciences 116, 103865. https://doi.org/10.1016/j.jsames.2022.103865

Samper, A., Quidelleur, X., Boudon, G., Le Friant, A., Komorowski, J.C., 2008. Radiometric dating of three large volume flank collapses in the Lesser Antilles Arc. Journal of Volcanology and Geothermal Research 176, 485–492. https://doi.org/10.1016/j.jvolgeores.2008.04.018

Santamaría, S., 2017. Catálogo de eventos volcánicos ocurridos en el Ecuador continental desde el Plioceno y análisis de la frecuencia eruptiva (Engineer memoir). Escuela Politécnica Nacional, Quito, Ecuador.

Santamaría, S., Quidelleur, X., Hidalgo, S., Samaniego, P., Le Pennec, J.-L., Liorzou, C., Lahitte, P., Córdova, M., Espín, P., 2022. Geochronological evolution of the potentially active Iliniza Volcano (Ecuador) based on new K-Ar ages. Journal of Volcanology and Geothermal Research 424, 107489. https://doi.org/10.1016/j.jvolgeores.2022.107489

Santamaría, S., Quidelleur, X., Samaniego, P., Audin, L., Le Pennec, J.-L., Hidalgo, S., Liorzou, C., Guillou, H., 2023. Timing of Quaternary volcanism and its relationship with tectonics in the central segment of the Ecuadorian Andes. Journal of Volcanology and Geothermal Research 442, 107895. https://doi.org/10.1016/j.jvolgeores.2023.107895

Santamaria, S., Quidelleur, X., Samaniego, P., Audin, L., Le Pennec, J.-L., Hidalgo, S., Liorzou, C., Guillou, H., 2023. Timing of Quaternary volcanism and its relationship with tectonics in the central segment of the Ecuadorian Andes. Journal of Volcanology and Geothermal Research 442, 107895. https://doi.org/10.1016/j.jvolgeores.2023.107895

Santamaría, S., Telenchana, E., Bernard, B., Hidalgo, S., Beate, B., Córdova, M., Narváez, D., 2017. Registro de erupciones ocurridas en los Andes del Norte durante el Holoceno: Nuevos resultados obtenidos en la turbera de Potrerillos, Complejo Volcánico Chiles-Cerro Negro. Revista Politécnica 39, 7–16.

Schaen, A.J., Jicha, B.R., Hodges, K.V., Vermeesch, P., Stelten, M.E., Mercer, C.M., Phillips, D., Rivera, T.A., Jourdan, F., Matchan, E.L., Hemming, S.R., Morgan, L.E., Kelley, S.P., Cassata, W.S., Heizler, M.T., Vasconcelos, P.M., Benowitz, J.A., Koppers, A.A.P., Mark, D.F., Niespolo, E.M., Sprain, C.J., Hames, W.E., Kuiper, K.F., Turrin, B.D., Renne, P.R., Ross, J., Nomade, S., Guillou, H., Webb, L.E., Cohen, B.A., Calvert, A.T., Joyce, N., Ganerød, M., Wijbrans, J., Ishizuka, O., He, H., Ramirez, A., Pfänder, J.A., Lopez-Martínez, M., Qiu, H., Singer, B.S., 2020. Interpreting and reporting 40Ar/39Ar geochronologic data. GSA Bulletin 133, 461–487. https://doi.org/10.1130/B35560.1

Schwarz, W.H., Trieloff, M., 2007. Intercalibration of 40Ar–39Ar age standards NL-25, HB3gr hornblende, GA1550, SB-3, HD-B1 biotite and BMus/2 muscovite. Chemical Geology 242, 218–231. https://doi.org/10.1016/j.chemgeo.2007.03.016

Singer, B.S., Wijbrans, J.R., Nelson, S.T., Pringle, M.S., Feeley, T.C., Dungan, M.A., 1998. Inherited argon in a Pleistocene andesite lava: 40Ar/39Ar incremental-heating and laser-fusion analyses of plagioclase. Geology 26, 427–430. https://doi.org/10.1130/0091-7613(1998)026<0427:IAIAPA>2.3.CO;2

Spikings, R., Cochrane, R., Villagomez, D., Van der Lelij, R., Vallejo, C., Winkler, W., Beate, B., 2015. The geological history of northwestern South America: from Pangaea to the early collision of the Caribbean Large Igneous Province (290–75Ma). Gondwana Research 27, 95–139. https://doi.org/10.1016/j.gr.2014.06.004

Steiger, R.H., Jäger, E., 1977. Subcommission on geochronology: Convention on the use of decay constants in geo- and cosmochronology. Earth and Planetary Science Letters 36, 359–362. https://doi.org/10.1016/0012-821X(77)90060-7

Sun, S.-S., McDonough, W.F., 1989. Chemical and isotopic systematics of oceanic basalts: implications for mantle composition and processes. Geol. Soc. Lond. Spec. Publ. 42, 313–345. https://doi.org/10.1144/GSL.SP.1989.042.01.19

Sychev, I.V., Koulakov, I., Egorushkin, I., Zhuravlev, S., West, M., Khrepy, S.E., Al-Arifi, N., Alajmi, M.S., 2019. Fault-Associated Magma Conduits Beneath Volcán de Colima Revealed by Seismic Velocity and Attenuation Tomography Studies. Journal of Geophysical Research: Solid Earth 124, 8908–8923. https://doi.org/10.1029/2019JB017449

Takada, A., 1994. The influence of regional stress and magmatic input on styles of monogenetic and polygenetic volcanism. Journal of Geophysical Research: Solid Earth 99, 13563–13573. https://doi.org/10.1029/94JB00494

Telenchana, E., Bernard, B., Hidalgo, S., Beate, B., 2017. Modelo evolutivo del volcán Chiles, in: Memorias VIII Jornadas En Ciencias de La Tierra. Presented at the 8vas Jornadas en Ciencias de la Tierra, pp. 391–395.

Tibaldi, A., Bonali, F.L., 2017. Intra-arc and back-arc volcano-tectonics: Magma pathways at Holocene Alaska-Aleutian volcanoes. Earth-Science Reviews 167, 1–26. https://doi.org/10.1016/j.earscirev.2017.02.004

Tibaldi, A., Bonali, F.L., Corazzato, C., 2017. Structural control on volcanoes and magma paths from local- to orogen-scale: The central Andes case. Tectonophysics 699, 16–41. https://doi.org/10.1016/j.tecto.2017.01.005

Tibaldi, A., Rovida, A., Corazzato, C., 2007. Late Quaternary kinematics, slip-rate and segmentation of a major Cordillera-parallel transcurrent fault: The Cayambe-Afiladores-Sibundoy system, NW South America. Journal of Structural Geology 29, 664–680. https://doi.org/10.1016/j.jsg.2006.11.008

Tsunematsu, K., Bonadonna, C., 2015. Grain-size features of two large eruptions from Cotopaxi volcano (Ecuador) and implications for the calculation of the total grain-size distribution. Bull Volcanol 77, 1–12. https://doi.org/10.1007/s00445-015-0949-4

Vallejo, C., Almagor, S., Romero, C., Herrera, J.L., Escobar, V., Spikings, R., Winkler, W., Vermeesch, P., 2020. Sedimentology, Provenance and Radiometric Dating of the Silante Formation: Implications for the Cenozoic Evolution of the Western Andes of Ecuador. Minerals 10, 929. https://doi.org/10.3390/min10100929

Vallejo, C., Romero, C., Horton, B.K., Spikings, R.A., Gaibor, J., Winkler, W., Esteban, J.J., Thomsen, T.B., Mariño, E., 2021. Jurassic to Early Paleogene sedimentation in the Amazon region of Ecuador: Implications for the paleogeographic evolution of northwestern South America. Global and Planetary Change 204, 103555. https://doi.org/10.1016/j.gloplacha.2021.103555

Vallejo, C., Spikings, R., Horton, B.K., Luzieux, L., Romero, C., Winkler, W., Thomsen, T.B., 2019. Chapter 8 - Late cretaceous to miocene stratigraphy and provenance of the coastal forearc and Western Cordillera of Ecuador: Evidence for accretion of a single oceanic plateau fragment, in: Horton, B.K., Folguera, A. (Eds.), Andean Tectonics. Elsevier, pp. 209–236. https://doi.org/10.1016/B978-0-12-816009-1.00010-1

Valverde, V., Mothes, P.A., Beate, B., Bernard, J., 2021. Enormous and far-reaching debris avalanche deposits from Sangay volcano (Ecuador): Multidisciplinary study and modeling the 30 ka sector collapse. Journal of Volcanology and Geothermal Research 411, 107172. https://doi.org/10.1016/j.jvolgeores.2021.107172

van Wyk de Vries, B., van Wyk de Vries, M., 2018. Chapter 7 - Tectonics and Volcanic and Igneous Plumbing Systems, in: Burchardt, S. (Ed.), Volcanic and Igneous Plumbing Systems. Elsevier, pp. 167–189. https://doi.org/10.1016/B978-0-12-809749-6.00007-8

Vezzoli, L., Apuani, T., Corazzato, C., Uttini, A., 2017. Geological and geotechnical characterization of the debris avalanche and pyroclastic deposits of Cotopaxi Volcano (Ecuador). A contribute to instability-related hazard studies. Journal of Volcanology and Geothermal Research 332, 51–70. https://doi.org/10.1016/j.jvolgeores.2017.01.004

Villagómez, D., 2003. Evolución geológica Plio cuaternaria del valle Interandino central en Ecuador zona Quito Guayllabamba San Antonio (Engineer memoir). Escuela Politécnica Nacional, Quito, Ecuador.

Villagómez, D., Spikings, R., Magna, T., Kammer, A., Winkler, W., Beltrán, A., 2011. Geochronology, geochemistry and tectonic evolution of the Western and Central cordilleras of Colombia. Lithos 125, 875–896. https://doi.org/10.1016/j.lithos.2011.05.003

Villares, F., 2010. Estudio geovulcanologico de la zona sur de la caldera Chacana, provincias de Napo - Pichincha (Engineer memoir). Escuela Politécnica Nacional, Quito, Ecuador.

Villares, F., Garcia-Casco, A., Blanco-Quintero, I.F., Montes, C., Reyes, P.S., Cardona, A., 2020. The Peltetec ophiolitic belt (Ecuador): a window to the tectonic evolution of the Triassic margin of western Gondwana. International Geology Review 0, 1–25. https://doi.org/10.1080/00206814.2020.1830313

Winkler, W., Villagómez, D., Spikings, R., Abegglen, P., Tobler, St., Egüez, A., 2005. The Chota basin and its significance for the inception and tectonic setting of the inter-Andean depression in Ecuador. Journal of South American Earth Sciences, Cenozoic Andean Basin Evolution 19, 5–19. https://doi.org/10.1016/j.jsames.2004.06.006

Witt, C., Bourgois, J., 2010. Forearc basin formation in the tectonic wake of a collision-driven, coastwise migrating crustal block: The example of the North Andean block and the extensional Gulf of Guayaquil-Tumbes Basin (Ecuador-Peru border area). GSA Bulletin 122, 89–108. https://doi.org/10.1130/B26386.1

Witt, C., Bourgois, J., Michaud, F., Ordoñez, M., Jiménez, N., Sosson, M., 2006. Development of the Gulf of Guayaquil (Ecuador) during the Quaternary as an effect of the North Andean block tectonic escape. Tectonics 25. https://doi.org/10.1029/2004TC001723

Witt, C., Reynaud, J.Y., Barba, D., Poujol, M., Aizprua, C., Rivadeneira, M., Amberg, C., 2019. From accretion to forearc basin initiation: The case of SW Ecuador, Northern Andes. Sedimentary Geology 379, 138–157. https://doi.org/10.1016/j.sedgeo.2018.11.009

Yamamoto, T., Kudo, T., Isizuka, O., 2018. Temporal variations in volumetric magma eruption rates of Quaternary volcanoes in Japan. Earth Planets Space 70, 1–12. https://doi.org/10.1186/s40623-018-0849-x

Yepes, H., Audin, L., Alvarado, A., Beauval, C., Aguilar, J., Font, Y., Cotton, F., 2016. A new view for the geodynamics of Ecuador: Implication in seismogenic source definition and seismic hazard assessment. Tectonics 35, 1249–1279. https://doi.org/10.1002/2015TC003941

FIGURES

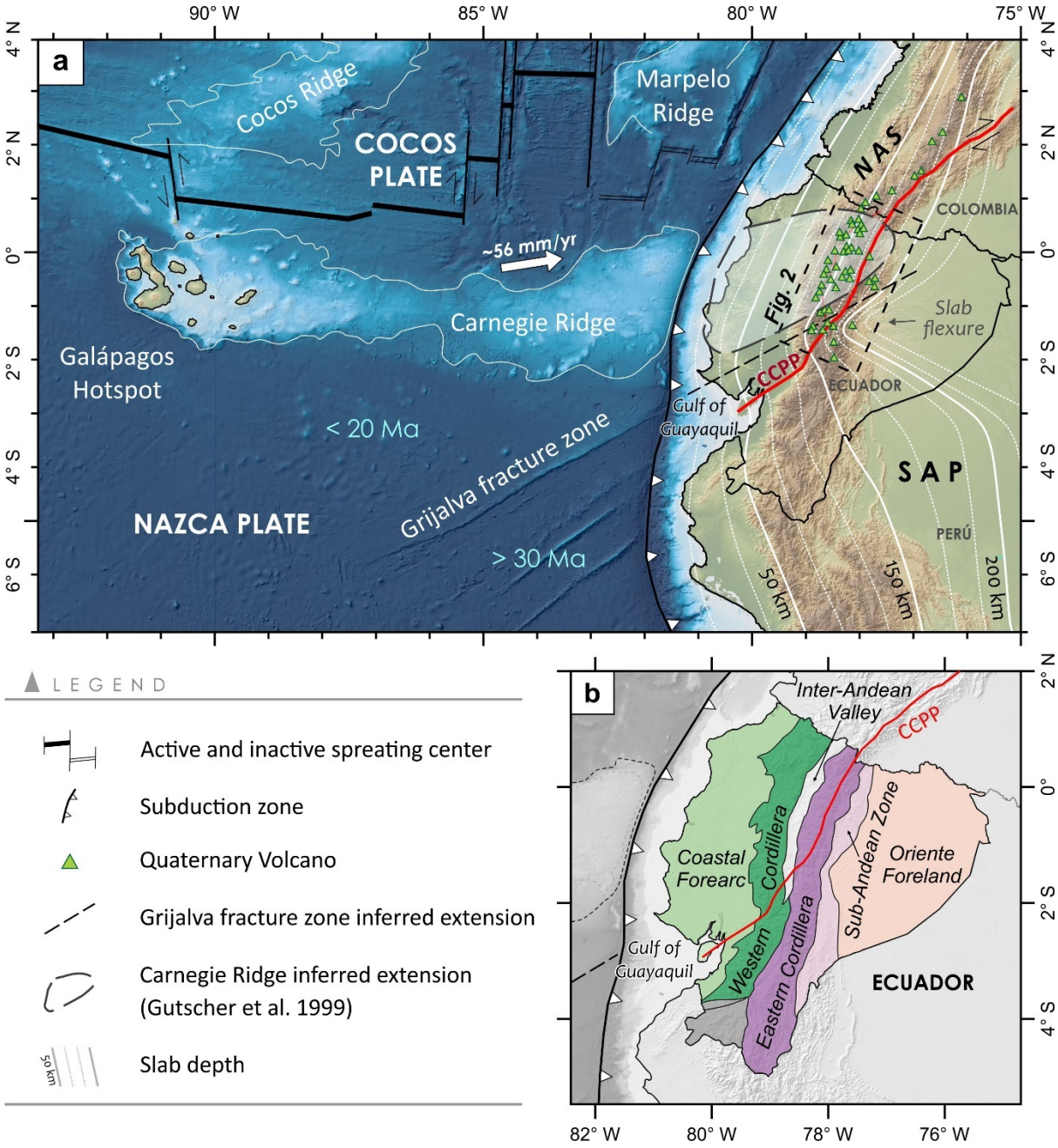

Figure 1. a) Geodynamic setting of the Ecuadorian margin. White arrow indicate the direction of the Nazca plate motion relative to South America (DeMets et al., 2010). Topography and bathymetry from the GEBCO 2020 program. Slab depth and Carnegie Ridge inferred extension from Yepes et al. (2016) and Gutscher et al. (1999), respectively. CCPP: Chingual-Cosanga-Pallatanga-Puná fault system (Alvarado et al., 2016). NAS: North Andean Sliver; SAP: South American Plate. **b)** Major geomorphological provinces of Ecuador (modified from Aspden et al., 1992).

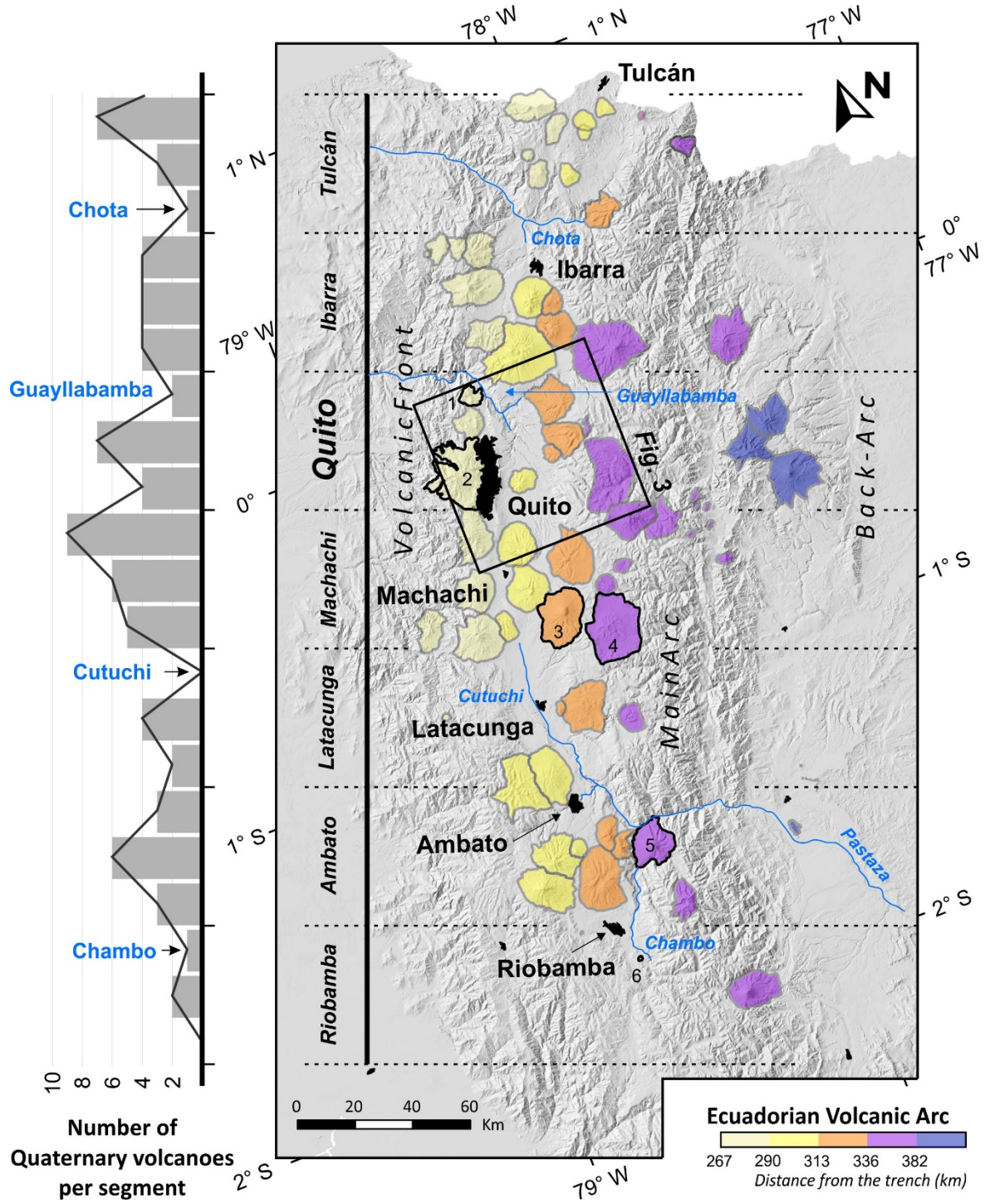

Figure 2. Segmentation of the Ecuadorian volcanic arc. Each section is named after the main city it contains, which are highlighted with black bold letters. Volcanoes' shapes taken from Bernard and Andrade (2011), and are colored according to their distance from the trench. Examples of volcanic landforms: (1) Pululahua lava dome complex, (2) Pichincha volcanic complex, (3) Cotopaxi volcano, (4) Chalupas caldera, (5) Tungurahua volcano, (6) Tulabug cone. Main valleys represented as blue letters.

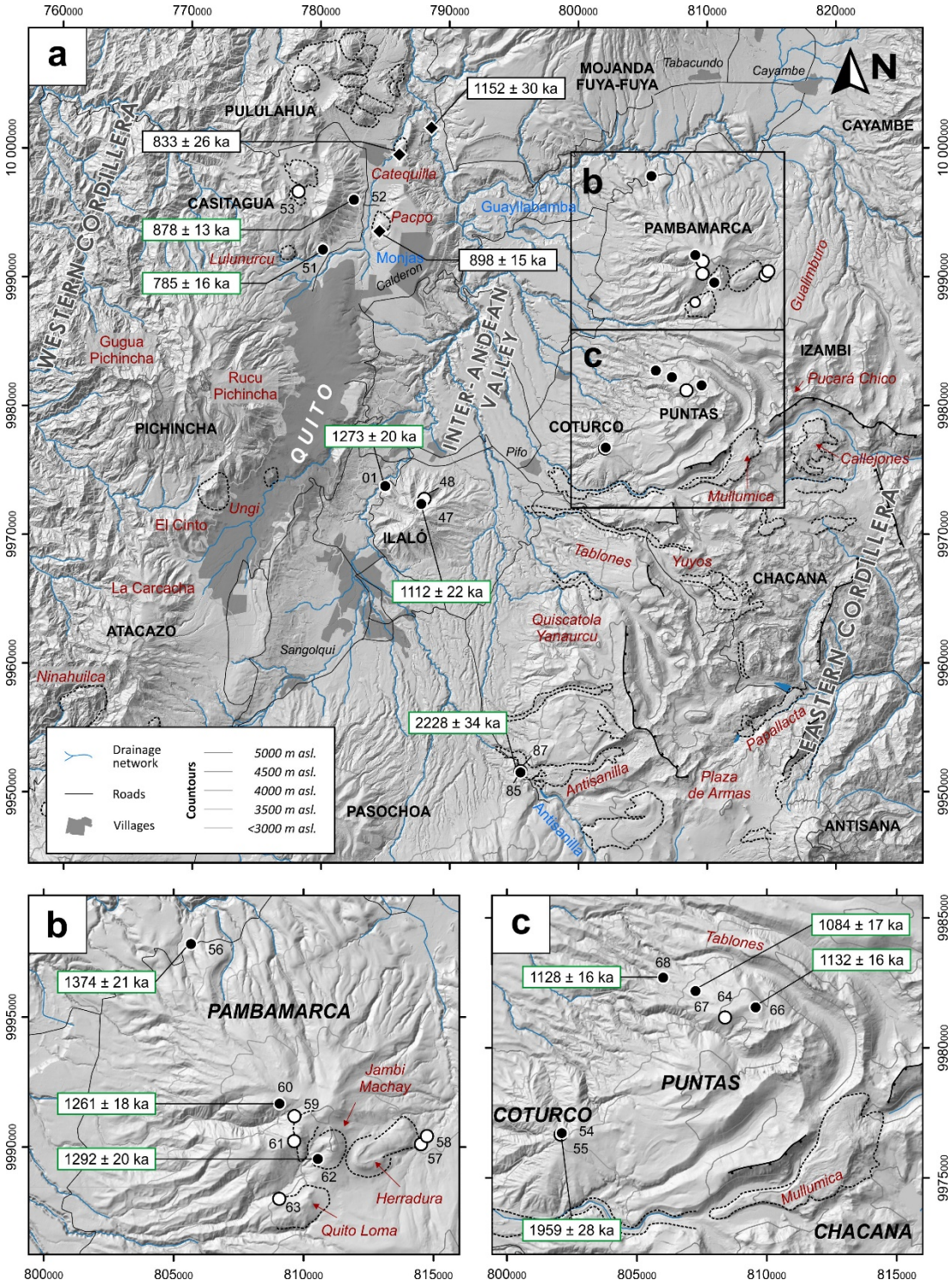

Figure 3. Hill-shaded digital surface model (topography from the Sigtierras program) of the Quito Segment showing the sampling locations and geochronological results. Numbers correspond to the last two digits of sample names (19EQxx or 20EQxx according to the recollection year). K-Ar dated samples are represented with solid symbols. K-Ar ages from Alvarado et al. (2014) are shown with black diamonds. Volcanoes shown as black bold letters. Volcanic landforms shown as red letters. Rivers and valleys represented as blue letters. Coordinates are in Universal Transverse Mercator (UTM) zone 17.

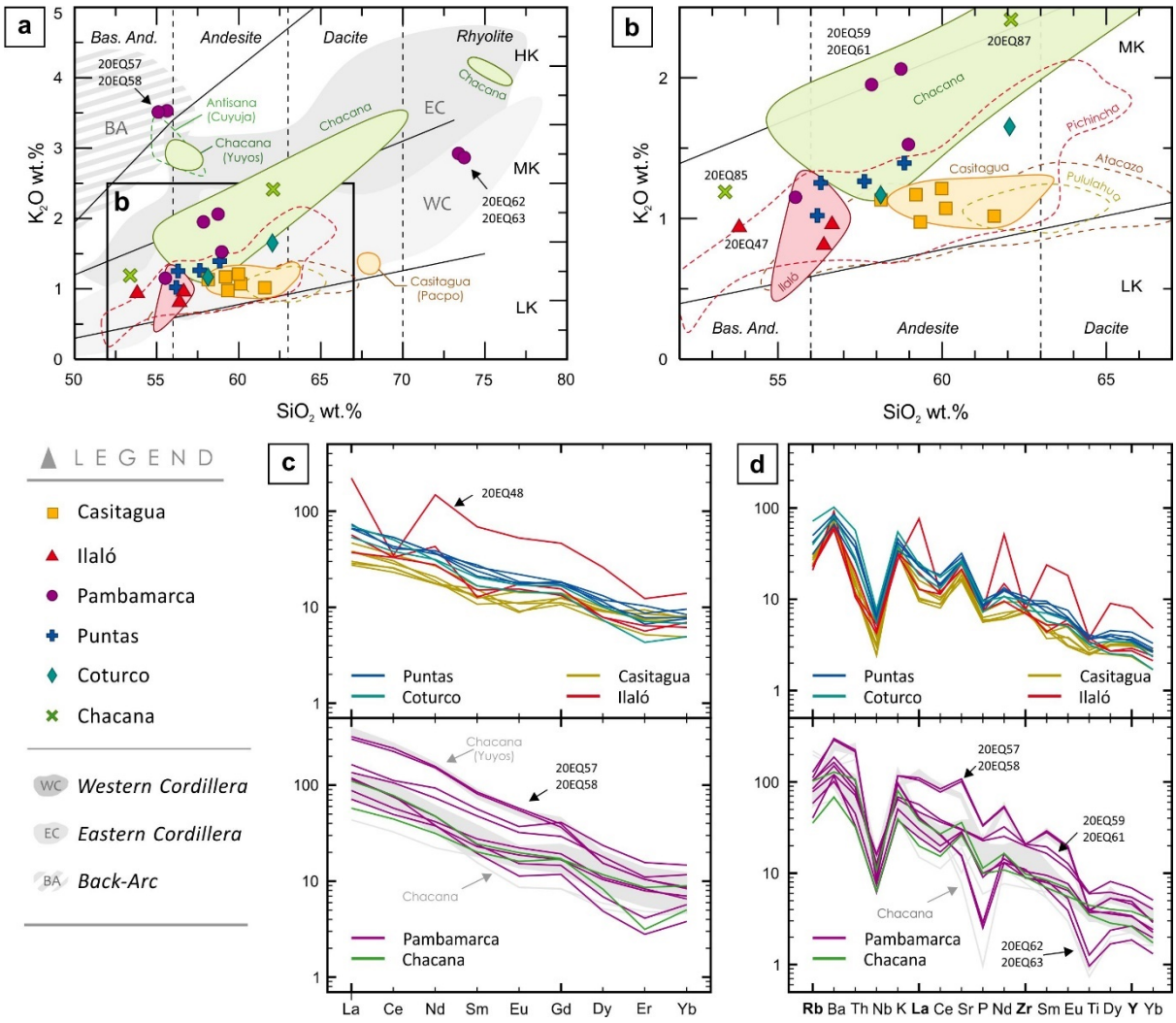

Figure 4. a-b) K_2O vs SiO_2 diagram (Peccerillo and Taylor, 1976) for eruptive products of the Quito segment volcanoes. HK: high-K, MK: medium-K, and LK: low-K calc-alkaline series. Colored areas represent the composition fields created by bibliographic data for Casitagua, Chacana, and Ilaló volcanoes (Pacheco, 2013; Chiaradia et al., 2009, 2014). Shaded areas represent the composition fields of the volcanoes from Western Cordillera, Eastern Cordillera, and Back-Arc based on the Georoc database (http://georoc.mpch-mainz.gwdg.de/georoc/). **c)** Rare Earth Elements normalized to chondrites, and **d)** Incompatible trace elements normalized to the primitive mantle diagrams (Sun and McDonough, 1989) for the Quito segment. The sampled volcanoes were organized according to their position in the Western Cordillera (yellow lines), Inter-Andean Valley (red lines), and Eastern Cordillera (blue and turquoise lines). Chacana (green lines) and Pambamarca (purple lines) samples showed in separated panels. Shaded area refers to bibliographic data from Chacana (Bryant et al., 2006; Chiaradia et al., 2009, 2014).

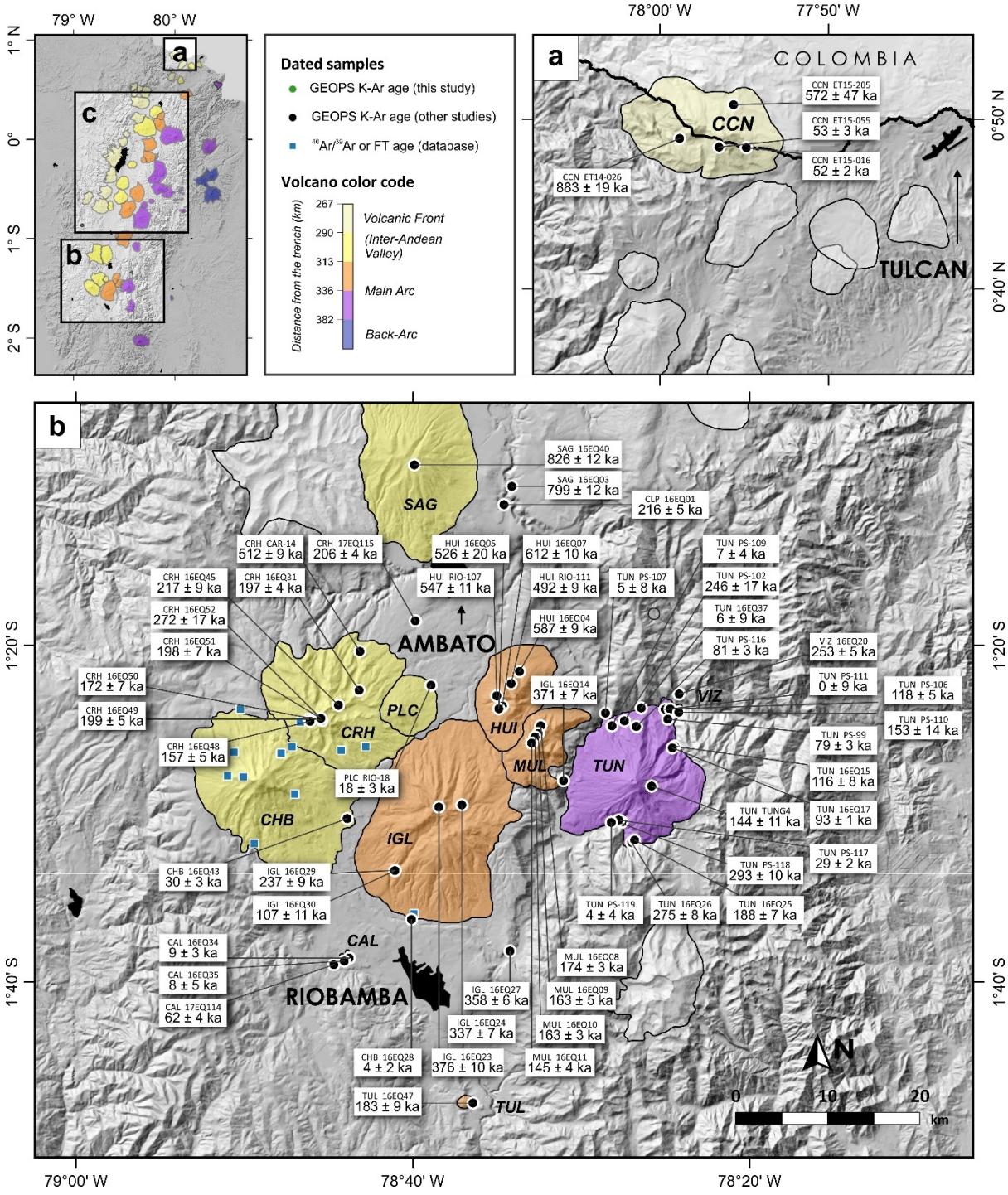

Figure 5. (Caption provided above)

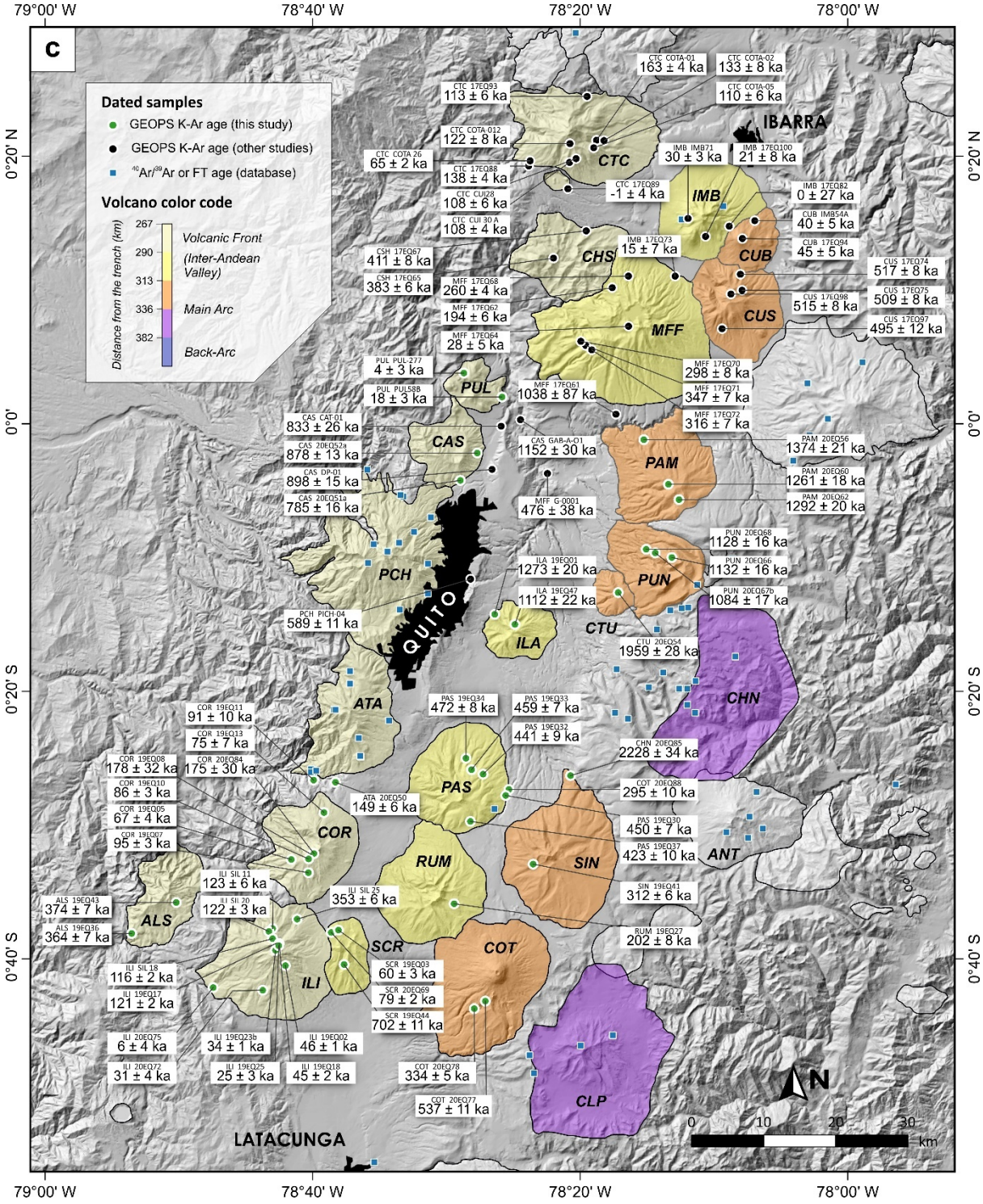

Figure 5. Summary of the location of published K-Ar, $^{40}Ar/^{39}Ar$ and obsidian Fission Track (FT) ages obtained on products of the current Ecuadorian arc, and of the new K-Ar ages presented in this study (black dots, blue squares, and green dots, respectively). Sampled volcanoes are colored in function to their distance to the trench. Details of the sampled unit, dated material, and references are available in Appendix C.

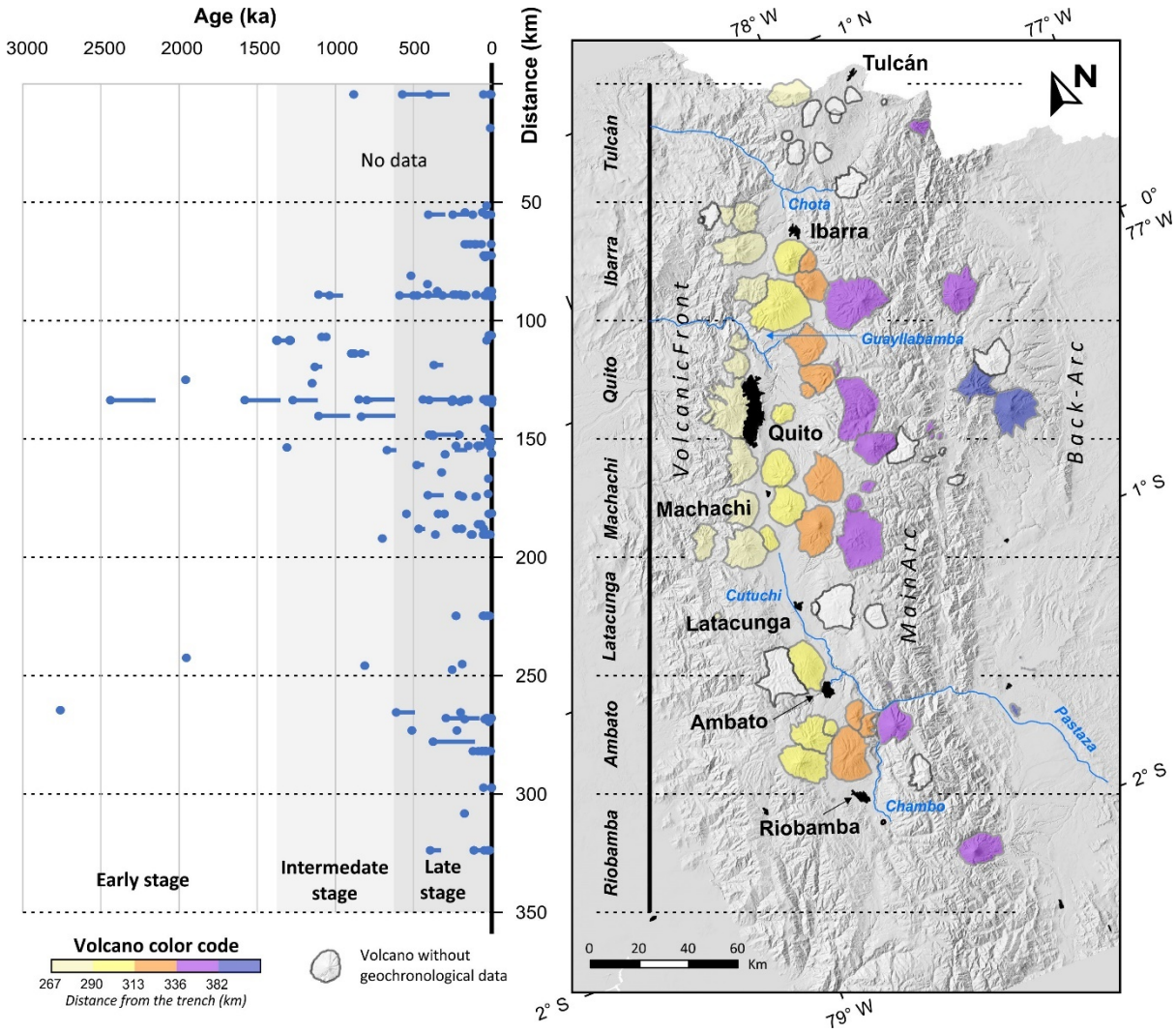

Figure 6. Stages of eruptive history of the Ecuadorian arc. Individual cone-building stages represented according to the position of each volcano relative to the Volcanic Front axis. The cone-building stages of a lifespan lest than ~100 kyr are represented as solid dots. The oldest stages of the volcanoes in the Tulcán and Latacunga segments remain poorly constrained.

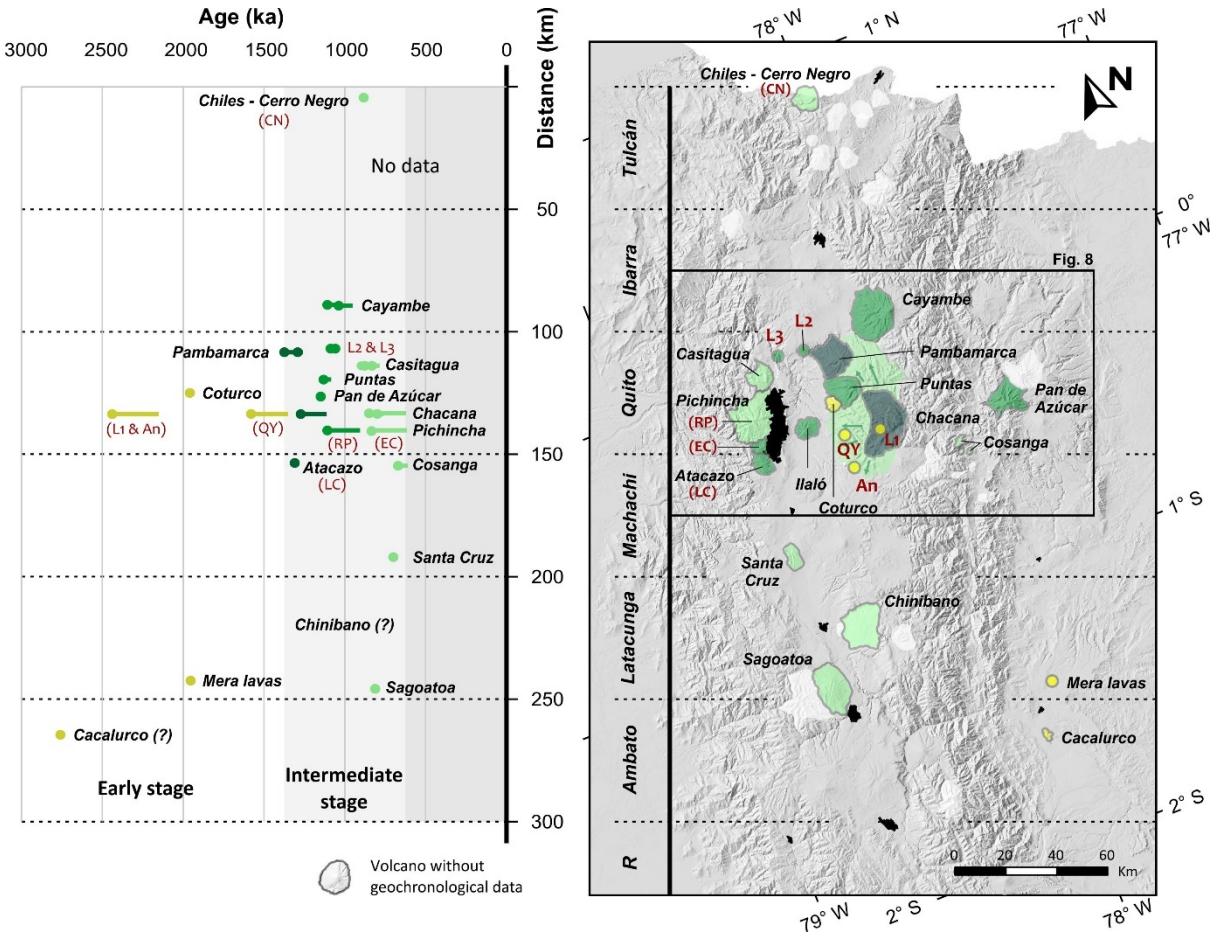

Figure 7. Sketch of the Early (dark yellow) and Intermediate (green) stages of eruptive history of the Ecuadorian arc. The structures crated during the Intermediate stage colored by age: 1.4-1.2 Ma (dark green), 1.2-1.0 Ma (green), and 1.0-0.6 Ma (light green). The locations of the Pre-Chacana (L1), Pre-Mojanda (L2), Pisque Fm (L3), and Mera eruptive centers are undefined, thus they are represented as oversized dots. Landforms referred in the text shown as red letters as in Figure 3. An: Antisanilla; EC: El Cinto; LC: La Carcacha; QY: Quiscatola-Yanaurcu series; RP: Rucu Pichincha.

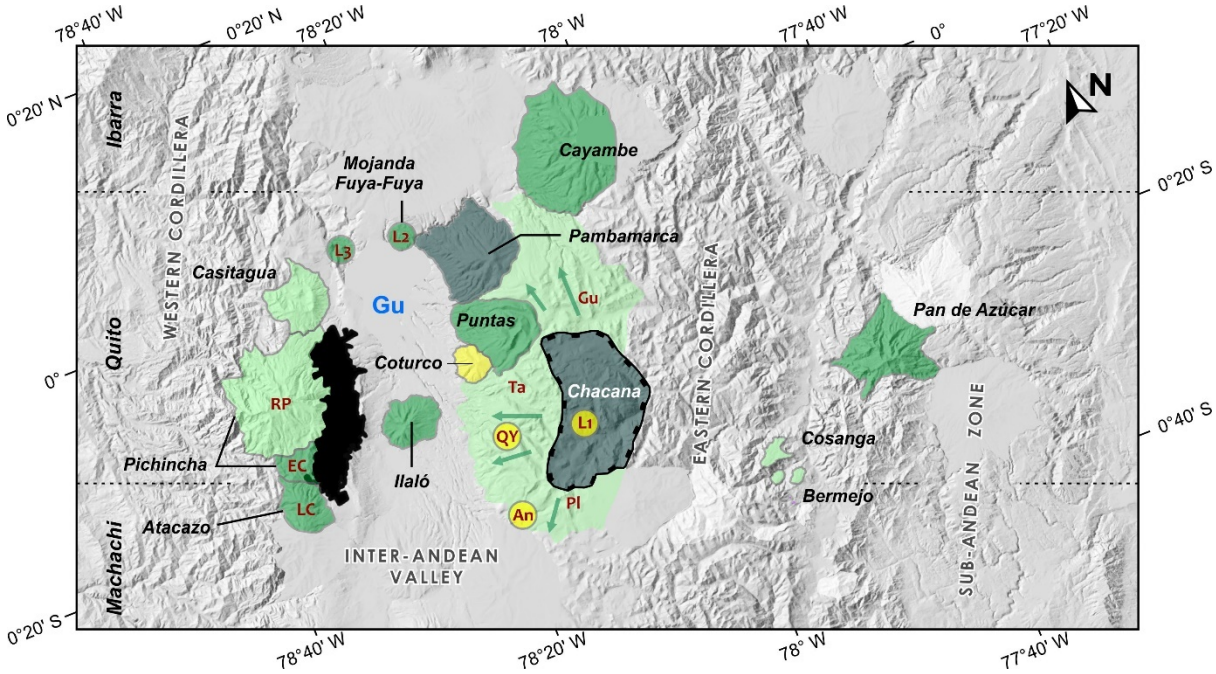

Figure 8. Sketch of the Quito segment at the end of the Intermediate stage. Volcanic landforms colored as in Figure 6. **Early stage events:** emission of the pre-Chacana lavas (L1, An, QY) and construction of the Coturco volcano. **Intermediate stage events:** formation of the early Chacana series followed by the construction of the Pambamarca, Puntas, and Viejo Cayambe edifices. Further east, construction of Ilaló, El Cinto (EC), and La Carcacha (LC), and emission of the Pre-Mojanda (L2) and Pisque (L3) lavas. Activity of Pan de Azúcar volcano occurred in the Sub-Andean zone. The last edifices to be constructed were Casitagua and Rucu Pichincha (RP). The deposits created by the formation of the Chacana Caldera (Gu, Ta, Pl) partially covered the Pambamarca, Puntas, and Coturco volcanoes.

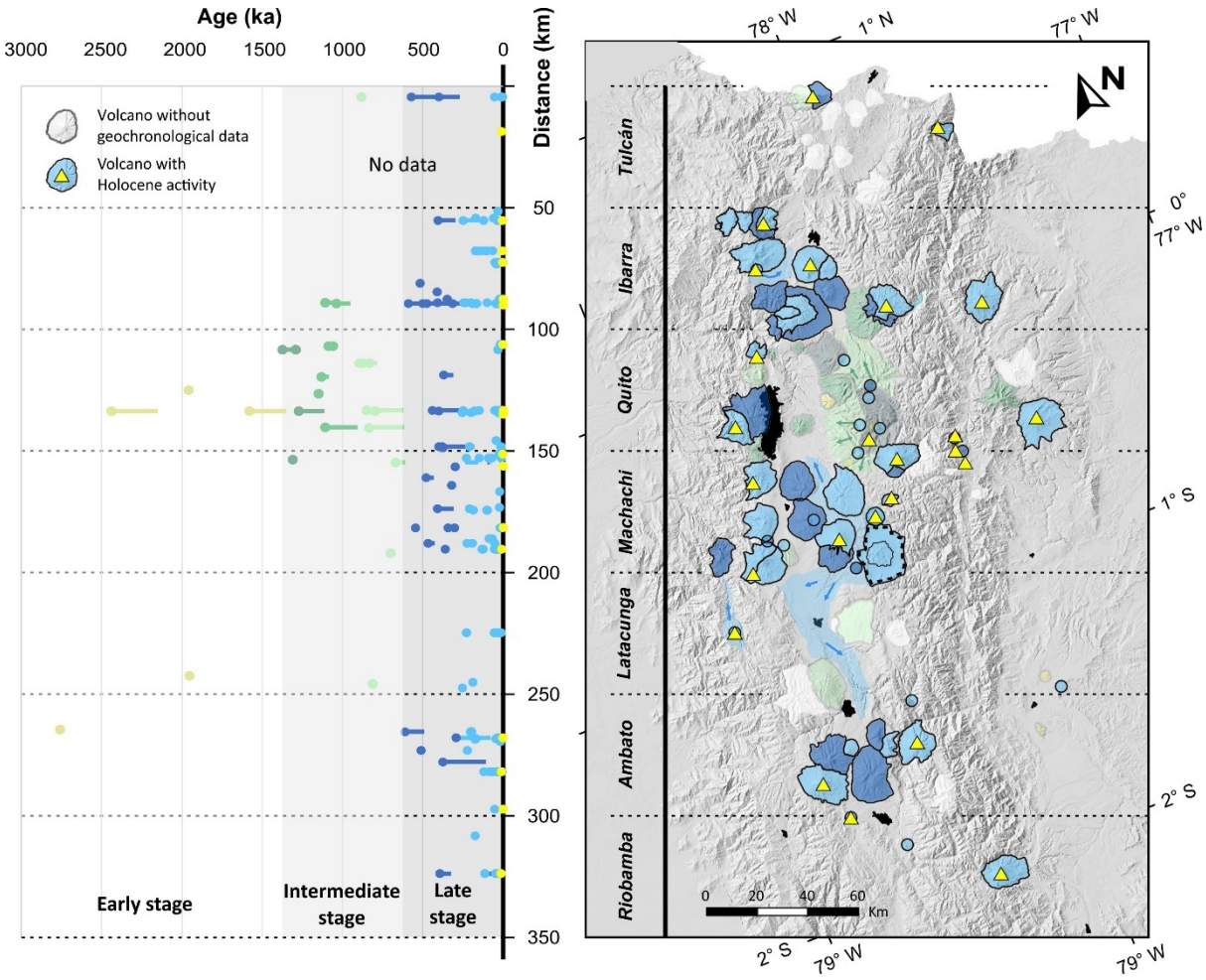

Figure 9. Sketch of the Late (blue) stage of the eruptive history of the Ecuadorian arc. Structures created during this stage colored by age: 600-300 ka (dark blue) and <300 ka (light blue). Locations of small eruptive centers (<5 km in diameter) represented as oversized dots. Volcanoes with Holocene activity highlighted with yellow triangles. See Appendix C for a detailed view and volcano names.

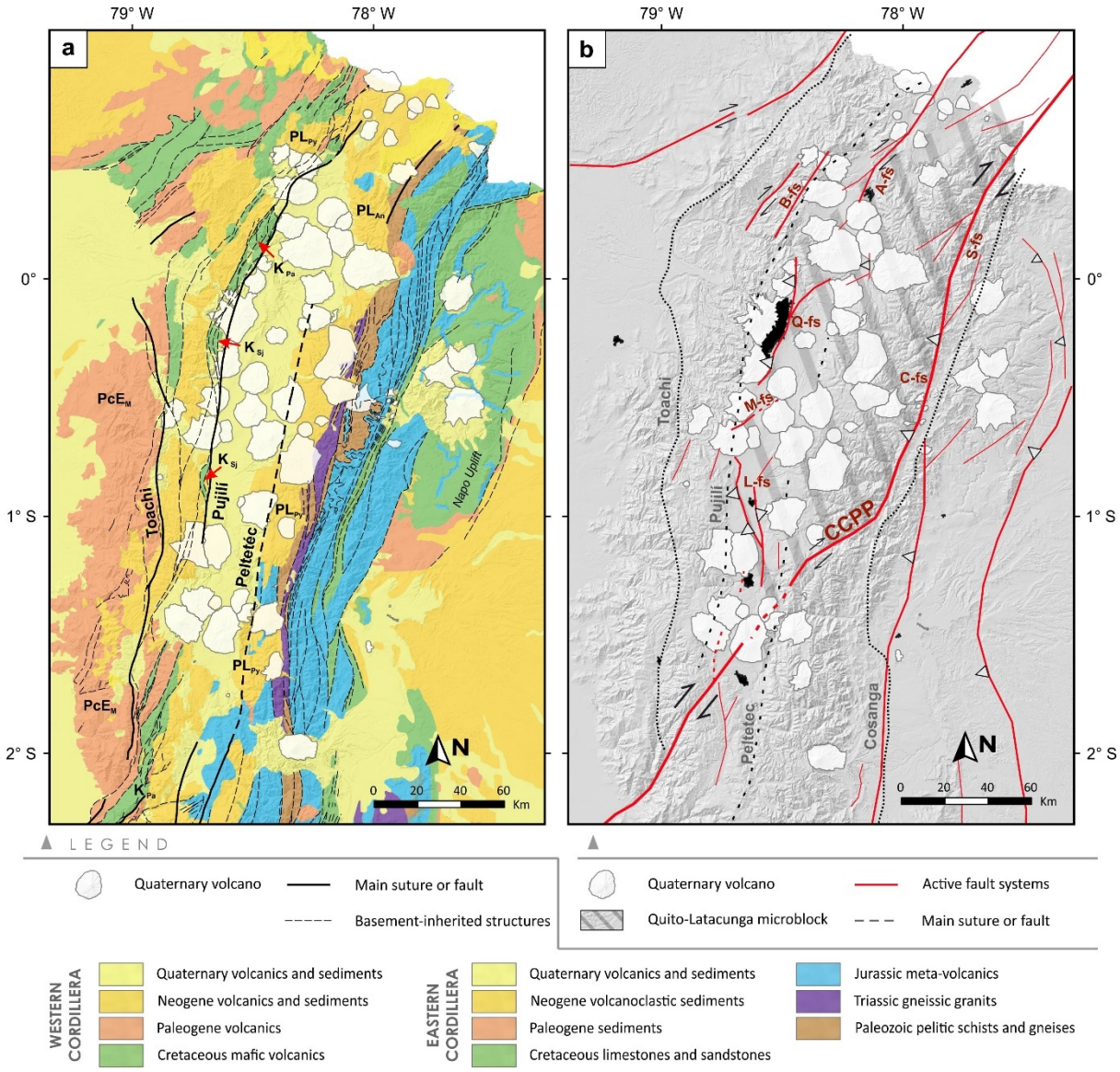

Figure 10. a) Simplified geological map of the central and northern Ecuadorian Andes showing the basement-inherited structures beneath the volcanic arc (Modified from Hughes and Bermúdez, 1997; Litherland et al., 1994; Egüez et al., 2017; Vallejo et al., 2019). Geological units mentioned in the text represented as black letters. PL_{An}: Angochagua; PcE_M: Macuchi; K_{Pa}: Pallatanga; PL_{Py}: Pizayambo; K_{Sj}: San Juan. b) Tectonic map of the same area describing the active faults as red lines. A-fs: Ambi; B-fs: Billecocha; C-fs: Cosanga; L-fs: Latacunga; M: Machachi; Q-fs: Quito; and S-fs: Salado fault systems as red letters.

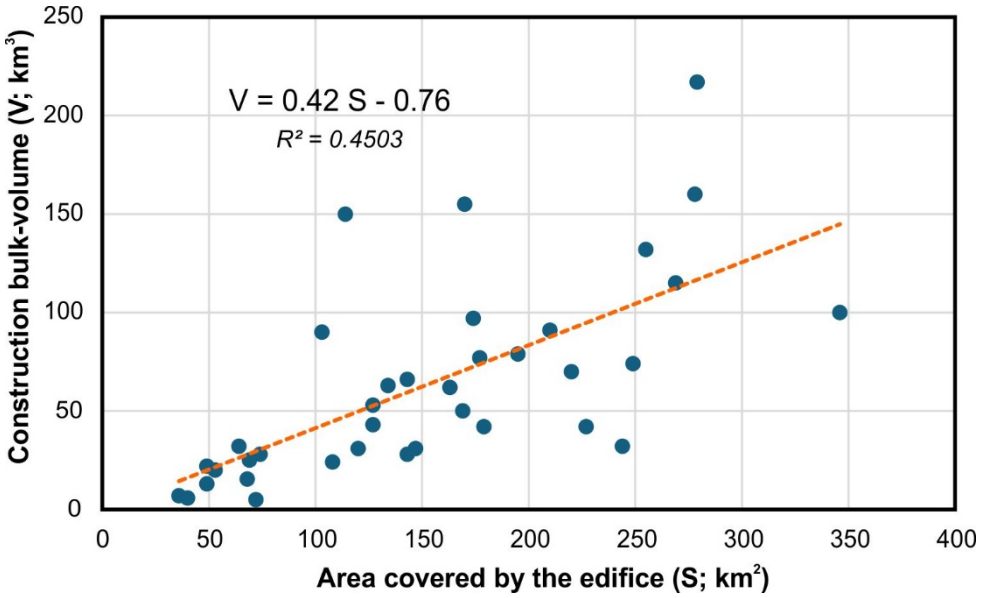

Figure 11. Correlation chart between construction bulk-volume (V; km^3) and area covered by the edifice (S; km^2) for the volcanoes of the Ecuadorian volcanic arc.

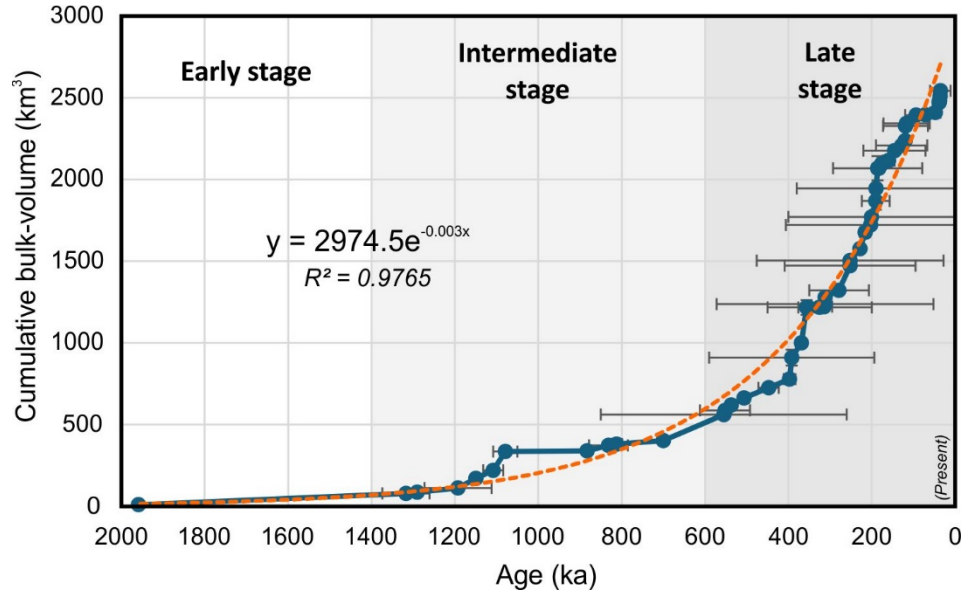

Figure 12. Cumulative construction bulk-volume (km^3) over time. Error bars on the x-axis reflect the estimated duration of the construction stages of each volcanic edifice. Error bars in the volume calculation (y-axis) are too small to be visible compared to the cumulative bulk-volume. The data used are given in Appendix D.

Table 1. New K-Ar ages obtained for the volcanoes of the Quito segment. Column headings indicate sample name, outcrop nature and relative location, sample coordinates projected using the Universal Transverse Mercator (UTM) coordinate system (Zone 17), potassium (K) content in percent, radiogenic argon content (^{40}Ar*) in percent and in 10^{11} atoms per gram, age obtained for each measurement, and weighted mean age in ka given with a 1-σ uncertainty. All measurements were performed on groundmass, except for three analyses performed on plagioclase phenocrysts (**).

Sample	Location and Unit	Longitude (m)	Latitude (m)	K (%)	^{40}Ar* (%)	^{40}Ar* (10^{11} at/g)	Age ± 1σ (ka)	Mean age (ka)
Casitagua volcano								
20EQ52a	Lava flow, E flank	782567	9995974	1.329	20.3	12.1227	873 ± 13	878 ± 13
					19.7	12.2556	883 ± 13	
20EQ51a	Lava flow, SE flank	780212	9992204	1.411	7.5	11.6027	787 ± 15	785 ± 16
					6.9	11.5223	782 ± 16	
Ilaló volcano								
19EQ01	Lava flow, E flank	784978	9973735	0.964	14.5	12.7775	1273 ± 20	1273 ± 20
					13.9	12.8238	1274 ± 20	
19EQ47	Lava flow, N flank	787784	9972350	1.133	7.1	12.9692	1096 ± 22	1112 ± 22
					7.1	13.2883	1123 ± 22	
					6.7	13.2122	1116 ± 23	
Pambamarca volcano								
20EQ56	Lava flow, NW flank	805673	9997815	1.241	19.5	17.804	1373 ± 21	1374 ± 21
					21.5	17.8125	1374 ± 20	
20EQ62**	Jambi Machay dome, summit area	810553	9989550	0.382	12.4	5.1262	1285 ± 21	1292 ± 20
					18.2	5.1773	1297 ± 20	
20EQ60	Lava flow, summit area	809077	9991663	1.586	37.2	20.7881	1254 ± 18	1261 ± 18
					39.2	21.0203	1268 ± 18	
Puntas volcano								
20EQ66	Lava flow, E flank	809562	9981566	1.449	31.7	17.0642	1127 ± 16	1132 ± 16
					33.2	17.2136	1137 ± 16	
20EQ68	Lava flow, E flank	806008	9982702	1.362	30.9	16.0579	1128 ± 16	1128 ± 16
					33.2	16.0570	1128 ± 16	
20EQ67b	Lava flow, E flank	807261	9982195	1.034	14.3	11.6670	1080 ± 17	1084 ± 17
					12.8	11.7687	1089 ± 18	
Coturco volcano								
20EQ54	Lava flow, summit area	802112	9976733	1.610	47.7	33.1602	1971 ± 28	1959 ± 28
20EQ54**				1.141	43.4	23.2191	1948 ± 28	
Chacana Caldera								
20EQ85	Lava flow, Antisanilla valley	795498	9951500	1.319	19.6	30.7537	2232 ± 34	2228 ± 34
					16.4	30.6488	2224 ± 34	

Table 2. Volcanic systems with radioisotopic ages. Segment refers to Figure 6. Oldest and youngest ages are given in ka. Volcanoes with a Holocene activity are considered as potentially active (Pot. Active); those with an historic activity or in eruption are considered as active (Bernard and Andrade, 2011); n.d.: not determined or unknown. Dating tech. (dating technique) and minerals used: wr (whole-rock), gms (groundmass), plg (plagioclase), obs (obsidian), FT (fission-tracks). References, 1: Bablon (2018); 2: Béguelin et al. (2015); 3: Bellver Baca et al. (2020); 4: Almeida et al. (2023); 5: Le Pennec et al. (2011); 6: Bablon et al. (2020a); 7: Samaniego et al. (2005); 8: Andrade et al. (2021): 9: Alvarado et al. (2014); 10: Robin et al. (2010); 11: Bigazzi et al. (1992); 12: Bigazzi et al. (2005); 13: Bellot-Gurlet et al. (2008); 14: Hoffer, (2008); 15: Hall et al. (2017); 16: Hidalgo (2006); 17: Santamaria et al. (2023); 18: Santamaria et al. (2022); 19: Hammersley (2003); 20: Opdyke et al. (2006); 21: Bablon et al. (2019); 22: Bablon et al. (2018); 23: Samaniego et al. (2022); 24: Hoffer et al. (2008); 25: Monzier et al. (1999).

Segment	Edifice - Abbreviation	Lat. (°N)	Long. (°E)	Oldest age (ka)	Youngest age (ka)	Dating tech.	Reference
Tulcan	Chiles - Cerro Negro - CCN	0.817	-77.936	883 ± 19	Pot. Active	K-Ar gms	1
Ibarra	Yanaurcu de Piñán - YNP	0.482	-78.33	3610 ± 60	61 ± 20	$^{40}Ar/^{39}Ar$ gms	2
Ibarra	Chachimbiro - CCB	0.467	-78.312	406 ± 20	Pot. Active	$^{40}Ar/^{39}Ar$ gms	3
Ibarra	Cotacachi - Cuicocha - CTC	0.361	-78.349	173 ± 4	Pot. Active	K-Ar gms	4
Ibarra	Imbabura - IMB	0.254	-78.181	47 ± 6	Pot. Active	$^{40}Ar/^{39}Ar$ wr; K-Ar gms	5; 6
Ibarra	Cubilche - CUB	0.230	-78.132	45 ± 5	n.d.	K-Ar gms	6
Ibarra	Cushnirumi - CHS	0.191	-78.328	411 ± 8	383 ± 6	K-Ar gms	6
Ibarra	Cusín - CUS	0.159	-78.148	517 ± 8	495 ± 12	K-Ar gms	6
Ibarra	Mojanda - Fuya Fuya - MFF	0.133	-78.293	1038 ± 87	28 ± 5	K-Ar gms	6
Ibarra	Cayambe - CAY	0.025	-77.988	409 ± 4	Active	$^{40}Ar/^{39}Ar$ wr	7
Quito	Pululahua - PUL	0.035	-78.466	18 ± 3	Pot. Active	K-Ar gms	8
Quito	Casitagua - CAS	-0.034	-78.479	1152 ± 30	785 ± 16	K-Ar gms	This study; 9
Quito	Pambamarca - PAM	-0.08	-78.209	1374 ± 21	1261 ± 18	K-Ar gms	This study
Quito	Pichincha - PCH	-0.176	78.6	1100 ± 10	Active	$^{40}Ar/^{39}Ar$ wr	10
Quito	Puntas - PUN	-0.188	-78.205	1132 ± 16	1084 ± 17	K-Ar gms	This study
Quito	Izambi - IZA	-0.193	-78.172	370 ± 60	n.d.	FT obs	11; 12
Quito	Coturco - STU	-0.211	-78.286	1959 ± 28	n.d.	K-Ar gms	This study

Quito	Chacana - CHN	-0.214	-78.185	2710 ± 190	Active	FT obs.; $^{40}Ar/^{39}Ar$ gms	11; 12; 13
Quito	Ilaló - ILA	-0.263	-78.419	1273 ± 20	1112 ± 22	K-Ar gms	This study
Quito	Pan de Azúcar - PDA	-0.432	-77.719	1150 ± 10	n.d.	$^{40}Ar/^{39}Ar$ wr	14
Quito	Antisana - ANT	-0.485	-78.143	378 ± 38	Pot. Active	$^{40}Ar/^{39}Ar$ gms	15
Machachi	Atacazo - ATA	-0.357	-78.619	1290 ± 10	Pot. Active	$^{40}Ar/^{39}Ar$ gms	16
Machachi	Pasochoa - PAS	-0.467	-78.481	472 ± 8	423 ± 10	K-Ar gms	17
Machachi	Corazón - COR	-0.531	-78.66	178 ± 32	67 ± 4	K-Ar gms	17
Machachi	Sincholagua - SIN	-0.538	-78.372	312 ± 6	n.d.	K-Ar gms	17
Machachi	Rumiñahui - RUM	-0.581	-78.507	202 ± 8	n.d.	K-Ar plg	17
Machachi	Almas Santas - ALS	-0.59	-78.854	374 ± 7	364 ± 7	K-Ar gms	17
Machachi	Cosanga - COS	-0.603	-77.991	670 ± 60	290 ± 20	FT obs	11ou 12
Machachi	Santa Cruz - SCR	-0.652	-78.633	702 ± 11	60 ± 3	K-Ar gms	18
Machachi	Iliniza - ILI	-0.663	-78.716	353 ± 6	Pot. Active	K-Ar gms	18
Machachi	Cotopaxi - COT	-0.681	-78.438	537 ± 11	Active	K-Ar obs	17
Machachi	Chalupas - CLP	-0.781	-78.329	459 ± 9	169 ± 1	$^{40}Ar/^{39}Ar$ plg	19
Latacunga	Chinibano - CNB	-0.959	-78.476	1670 ± 190	n.d.	$^{40}Ar/^{39}Ar$ gms	20
Latatcunga	Sagoatoa - SAG	-1.155	-78.669	826 ± 12	799 ± 12	K-Ar gms	21
Ambato	Vizcaya - VIZ	-1.369	-78.414	253 ± 5	n.d.	K-Ar gms	22
Ambato	Puñalica - PLC	-1.399	-78.678	18 ± 3	n.d.	K-Ar gms	21
Ambato	Huisla - HUI	-1.4	-78.572	612 ± 10	492 ± 9	K-Ar gms	21
Ambato	Carihuairazo - CRH	-1.408	-78.751	512 ± 9	157 ± 5	K-Ar gms	23; 21
Ambato	Mera lavas - MER	-1.408	-77.927	2670 ± 60	1920 ± 100	$^{40}Ar/^{39}Ar$ wr	24
Ambato	Mulmul - MUL	-1.438	-78.543	174 ± 3	145 ± 4	K-Ar gms	21
Ambato	Puyo cones - PUY	-1.46	-77.914	190 ± 70	n.d.	$^{40}Ar/^{39}Ar$ wr	24
Ambato	Chimborazo - CHB	-1.467	-78.817	87 ± 8	Pot. Active	$^{40}Ar/^{39}Ar$ gms - K/Ar gms	23; 21
Ambato	Tungurahua - TUN	-1.47	-78.444	293 ± 10	Active	K-Ar gms	22
Ambato	Igualata - IGL	-1.493	-78.641	376 ± 10	107 ± 11	K-Ar gms	21
Riobamba	Calpi cones - CAL	-1.638	-78.731	62 ± 4	Pot. Active	K-Ar gms	21

Riobamba	Licto cones	-1.7837	-78.615	183 ± 9	n.d.	K-Ar gms	21
Riobamba	Sangay - SAN	-2.005	-78.342	380 ± 70	Active	$^{40}Ar/^{39}Ar$ gms	25